AFRL-ML-WP-TP-2007-407

LARGE CONCENTRATION-DEPENDENT NONLINEAR OPTICAL RESPONSES OF STARBURST DIPHENYLAMINO-FLUORENOCARBONYL METHANO[60]FULLERENCE PENTAADS (PREPRINT)

Hendry I. Elim, Wei Ji, Robinson Anandakathir, Long Y. Chiang, Rachel Jakubiak, and Loon-Seng Tan

OCTOBER 2006

Approved for public release; distribution unlimited.

STINFO COPY

MATERIALS AND MANUFACTURING DIRECTORATE
AIR FORCE RESEARCH LABORATORY
AIR FORCE MATERIEL COMMAND
WRIGHT-PATTERSON AIR FORCE BASE, OH 45433-7750

NOTICE AND SIGNATURE PAGE

Using Government drawings, specifications, or other data included in this document for any purpose other than Government procurement does not in any way obligate the U.S. Government. The fact that the Government formulated or supplied the drawings, specifications, or other data does not license the holder or any other person or corporation; or convey any rights or permission to manufacture, use, or sell any patented invention that may relate to them.

This report was cleared for public release by the Air Force Research Laboratory Wright Site (AFRL/WS) Public Affairs Office and is available to the general public, including foreign nationals. Copies may be obtained from the Defense Technical Information Center (DTIC) (http://www.dtic.mil).

AFRL-ML-WP-TP-2007-407 HAS BEEN REVIEWED AND IS APPROVED FOR PUBLICATION IN ACCORDANCE WITH ASSIGNED DISTRIBUTION STATEMENT.

*//Signature//

LOON-SENG TAN, Program Manager
Polymers Branch
Nonmetallic Materials Division

//Signature//

JOHN F. MAGUIRE, Chief
Polymers Branch
Nonmetallic Materials Division

//Signature//

SHASHI K. SHARMA, Acting Deputy Chief
Nonmetallic Materials Division
Materials and Manufacturing Directorate

This report is published in the interest of scientific and technical information exchange, and its publication does not constitute the Government's approval or disapproval of its ideas or findings.

*Disseminated copies will show "//Signature//" stamped or typed above the signature blocks.

REPORT DOCUMENTATION PAGE

Form Approved
OMB No. 0704-0188

1. REPORT DATE *(DD-MM-YY)*	2. REPORT TYPE	3. DATES COVERED *(From - To)*
October 2006	Journal Article Preprint	

4. TITLE AND SUBTITLE

LARGE CONCENTRATION-DEPENDENT NONLINEAR OPTICAL RESPONSES OF STARBURST DIPHENYLAMINOFLUORENOCARBONYL METHANO[60]FULLERENCE PENTAADS (PREPRINT)

5a. CONTRACT NUMBER
FA9950-05-0154

5b. GRANT NUMBER

5c. PROGRAM ELEMENT NUMBER
N/A

6. AUTHOR(S)

Hendry I. Elim and Wei Ji (National University of Singapore)
Robinson Anandakathir and Long Y. Chiang (University of Massachusetts Lowell)
Rachel Jakubiak and Loon-Seng Tan (AFRL/MLBP)

5d. PROJECT NUMBER
N/A

5e. TASK NUMBER
N/A

5f. WORK UNIT NUMBER
N/A

7. PERFORMING ORGANIZATION NAME(S) AND ADDRESS(ES)

National University of Singapore
Department of Physics
2 Science Drive 3
Singapore 117542, Singapore

University of Massachusetts
Department of Chemistry Lowell
Lowell, MA 01854

Polymers Branch (AFRL/MLBP)
Nonmetallic Materials Division
Materials and Manufacturing Directorate
Air Force Research Laboratory
Air Force Materiel Command
Wright-Patterson Air Force Base, OH 45433-7750

8. PERFORMING ORGANIZATION REPORT NUMBER

9. SPONSORING/MONITORING AGENCY NAME(S) AND ADDRESS(ES)

Materials and Manufacturing Directorate
Air Force Research Laboratory
Air Force Materiel Command
Wright-Patterson AFB, OH 45433-7750

10. SPONSORING/MONITORING AGENCY ACRONYM(S)
AFRL-ML-WP

11. SPONSORING/MONITORING AGENCY REPORT NUMBER(S)
AFRL-ML-WP-TP-2007-407

12. DISTRIBUTION/AVAILABILITY STATEMENT
Approved for public release; distribution unlimited.

13. SUPPLEMENTARY NOTES
Journal article submitted to the Journal of Materials Chemistry.
The U.S. Government is joint author of this work and has the right to use, modify, reproduce, release, perform, display, or disclose the work. PAO Case Number: AFRL/WS 06-2659, 01 Nov 2006.

14. ABSTRACT

We demonstrated an approach toward the design of starburst C_{60}-*keto*-DPAF assembly by applying a combination of a starburst macromolecular configuration with C_{60} as the core center, which is encapsulated by multiple bulky groups leading to the increase of intermolecular separation and aggregation barrier. Molecular compositions of the resulting C_{60}(>DPAF-C_9)$_2$ triad and C_{60}(>DPAF-C_9)$_4$ pentads were clearly confirmed by MALDI−MS (positive ion) detection of protonated molecular mass ions. Both C_{60}(>DPAF-C_9)$_2$ **2** and C_{60}(>DPAF-C_9)$_4$ (structural isomers, **3a** and **3b**) exhibited nonlinear optical transmittance reduction responses in femtosecond (fs) region with a lower transmittance % value for the latter at the high laser power above 80 GW/cm^2. It was attributed to larger fs 2PA cross-section values of **3a** and **3b** than that of **2** in the same concentration and, apparently, correlated to a higher number of DPAF-C_9 subunits in the structure of **3**. As the concentration was decreased to 10^{-4} M, a clear monotonous increase of the σ_2 value change ($\Delta\sigma_2$) in a quantity from 13.9, 33.2, to 48.1 and 68.2 × 10^{-48} cm4.sec.photon^{-1}.molecule^{-1} for the structural variation from the monoadduct **1**, bisadduct **2**, to tetraadducts **3**b and **3a**, respectively, was observed. We interpreted the concentration-dependent phenomena by the high tendency of fullerene-DPAF chromophores to form nanoscaled aggregates in a concentration above 10^{-3} M. We also proposed that starburst structures, as exemplified by C_{60}(>DPAF-C_9)4, in a multipolar arrangement resembling encapsulation of C_{60} by DPAF-C_9 pendants, provide a useful means to increase the degree of molecular dispersion and maintain high nonlinear optical efficiency.

15. SUBJECT TERMS
Starburst, C_{60}, ions, femtosecond (fs), DPAF

16. SECURITY CLASSIFICATION OF:			17. LIMITATION OF ABSTRACT:	18. NUMBER OF PAGES	19a. NAME OF RESPONSIBLE PERSON (Monitor)
a. REPORT	b. ABSTRACT	c. THIS PAGE			Loon-Seng Tan
Unclassified	Unclassified	Unclassified	SAR	38	19b. TELEPHONE NUMBER *(Include Area Code)* N/A

Standard Form 298 (Rev. 8-98)
Prescribed by ANSI Std. Z39-18

Large concentration-dependent nonlinear optical responses of starburst diphenylaminofluorenocarbonyl methano[60]fullerene pentaads

Hendry I. Elim,[a] Robinson Anandakathir,[b] Rachel Jakubiak,[c] Long Y. Chiang,*[b] Wei Ji,*[a] and Loon-Seng Tan*[c]

[a] *Department of Physics, National University of Singapore, 2 Science Drive 3, Singapore 117542, Singapore, E-mail: phyjiwei@nus.edu.sg; Fax: 65-67776126; Tel: 65-68742664*

[b] *Department of Chemistry, University of Massachusetts Lowell, Lowell, MA 01854, USA. E-mail: Long_Chiang@uml.edu; Fax: (978)-934-3013; Tel: (978)-934-3663*

[c] *Air Force Research Laboratory, AFRL/MLBP, Wright-Patterson Air Force Base, Dayton, OH 45433, USA. E-mail: Loon-Seng.Tan@wpafb.af.mil; Fax: (937)-255 -9157; Tel: (937)-255-9141*

Abstract

We demonstrated an approach toward the design of starburst C_{60}-*keto*-DPAF assembly by applying a combination of a starburst macromolecular configuration with C_{60} as the core center, which is encapsulated by multiple bulky groups leading to the increase of intermolecular separation and aggregation barrier. Molecular compositions of the resulting C_{60}(>DPAF-C_9)$_2$ triad and C_{60}(>DPAF-C_9)$_4$ pentads were clearly confirmed by MALDI–MS (positive ion) detection of protonated molecular mass ions. Both C_{60}(>DPAF-C_9)$_2$ **2** and C_{60}(>DPAF-C_9)$_4$ (structural isomers, **3a** and **3b**) exhibited nonlinear optical transmittance reduction responses in femtosecond (fs) region with a lower transmittance % value for the latter at the high laser power above 80 GW/cm^2. It was attributed to larger fs 2PA cross-section values of **3a** and **3b** than that of **2** in the same concentration and, apparently, correlated to a higher number of DPAF-C_9 subunits in the structure of **3**. As the concentration was decreased to 10^{-4} M, a clear monotonous increase of the σ_2 value change ($\Delta\sigma_2$) in a quantity from 13.9, 33.2, to 48.1 and 68.2 × 10^{-48} cm^4.sec.photon^{-1}.molecule^{-1} for the structural variation from the monoadduct **1**, bisadduct **2**, to tetraadducts **3b** and **3a**, respectively, was observed. We interpreted the concentration-dependent phenomena by the high tendency of fullerene-DPAF chromophores to form nanoscaled aggregates in a

concentration above 10^{-3} M. We also proposed that starburst structures, as exemplified by C_{60}(>DPAF-C_9)$_4$, in a multipolar arrangement resembling encapsulation of C_{60} by DPAF-C_9 pendants, provide a useful means to increase the degree of molecular dispersion and maintain high nonlinear optical efficiency.

Introduction

Chemical functionalization of C_{60} with organic groups to produce the corresponding monoadducts and bisadducts by converting one or two fullerenyl double bonds into two or four, respectively, sp^3 carbons, in general, does not alter much the overall π-conjugation and photophysical properties of the fullerene cage.[1–3] In fact, the covalent modification of C_{60} disrupts its symmetry-forbidden transitions and allows more ground state optical absorption in the visible region. Certain structural alteration given the formation of hexaarmed hydrophilic fullerene cage, such as that of FC_4S molecules, was proven to allow the extension of fullerenyl photoactivation processes to occur in the long wavelength region. Examples of their uses in the singlet oxygen generation,[4] photodynamic therapeutic fibrosacoma tumor treatment,[5] and photodynamic antibacterial coatings[6] with the application of a red-light laser source. Significant quantity of singlet oxygen produced by FC_4S implied the existence of photoinduced triplet excited transient state ($^3C_{60}$*) upon irradiation. This observation supports our hypothesis that the attachment of a limit number (≤ 6) of addends onto C_{60} forming a starburst molecular structure may not adversely affect its ability to form excited triplet fullerene state, which is considered to be one of crucial prerequisites for the reverse saturable absorption (RSA) and optical limiting properties of C_{60}-derived materials.[7–9] It is related to the well-recognized fact that excited states of C_{60} are more polarizable with larger absorption cross-section than those of ground states. Nearly co-existence of fullerenyl singlet and triplet excited states fits well with required facile generation of populated excited states for obtaining strong nonlinear optical responses[10] and the enhanced excited state absorption.[7,11] These RSA properties have been applied as the fundamental principle in the development of effective materials for protection from high-intensity laser pulses.[12–21]

Nonlinear absorption behavior of C_{60} appeared to be dominated by the reverse saturable absorption in the visible region and the two-photon absorption (2PA) process in the NIR-IR region.[22–24] Recently, large enhancement of molecular 2PA cross-sections in NIR region has been achieved by periconjugation of C_{60} with conjugated chromophores or grafted polymers.[25–29] One typical example of such conjugated chromophores was given by 9,9-diethyldiphenylaminofluorene (DPAF-C_2) which produces fluorescence emission centered at 498 nm in $CHCl_3$ upon excitation (~400 nm) near the ground state optical absorption peak maximum.[30] The emission is efficiently quenchable by C_{60} intermolecularly in a

solution mixture of methano[60]fullerene and DPAF-C_n or intramolecularly in the case of conjugated molecule, C_{60}(>DPAF-C_2), via energy transfer in nonpolar solvents, such as toluene, benzene, and CS_2. This energy transfer is plausible since the lowest excited singlet energy of C_{60}(>^{1}DPAF*-C_2) and $^1C_{60}$* (>DPAF-C_2) was estimated to be 2.74 (452 nm) and 1.74 (714 nm) eV, respectively, in toluene based on steady state fluorescence measurements.[31] The formation of fullerene triplet state was evident from the detection of triplet-triplet absorption band of $^3C_{60}$*(>DPAF-C_2) at about 730 nm in nanosecond transient absorption measurements after 532 nm laser irradiation, in close resemblance to that of parent C_{60} occurring at 750 nm upon similar excitation.[32] Therefore, photoexcitation of C_{60}(>DPAF-C_n) by 780 nm irradiation with respect to nearly a half of DPAF-C_n's HOMO-LUMO energy gap should facilitate both two-photon absorption of DPAF-C_n moiety and excited state absorption of fullerene moiety in a similar wavelength range. Combination of two-photon absorption and $^3C_{60}$* absorption in a nearly concurrent event may largely increase the overall nonlinear optical absorption capability of the materials in the ns time scale, in line with the proposed concept of the 2PA–RSA combination at the excited states of complex chromophores toward the reduction optical transmittance at high irradiance.[33–36] Accordingly, transient absorption data obtained from femtosecond pump-probe experiments at 800 nm on the samples of sterically hindered [60]fullerenyl dyad C_{60}(>DPAF-C_9) **1** and triads C_{60}(>DPAF-C_9)$_2$ **2**, where C_9 is 3,5,5-trimethylhexyl, unambiguously verified the occurrence of two-photon excitation processes in air-saturated benzene and subsequent efficient energy transfer from the two-photon pumped DPAF-C_9 moiety to the C_{60} cage moiety.[28] A similar study on C_{60}(>DPAF-C_9)$_2$ in CS_2 (1.0×10^{-2} M) also indicated good intrinsic fs 2PA cross-sections in the value of 0.824×10^{-48} cm^4.sec.photon^{-1}.molecule^{-1} (or 82.4 GM).

Synthetically, C_{60}-DPAF conjugates can be modified to further increase the number of chromophore arms on a single C_{60} cage resulting in a starburst structure for enhancing 2PA cross-sections. In this structural motif, the C_{60} cage serves as a molecular core for attaching multiple 2PA-active chromophore antenna components to harvest light in visible–NIR wavelength ranges and, subsequently, condense the excited-state energy to the central fullerene core. The approach resembles photoresponsive dendritic chromophore structures synthesized recently that embodied the fluorescence resonance energy transfer (FRET) phenomena.[37] Here, we report the first concentration-dependent 2PA cross-section measurements on starburst hindered diphenylaminofluorenocarbonyl methano[60]fullerene pentads C_{60}(>DPAF-C_9)$_4$ **3** and the observed significant decrease of relative 2PA cross-section values, especially, in a high solution concentration (10^{-2} M). In this concentration range, high tendency of intermolecular clustering and nano-aggregative interactions of this class of materials is believed to exist.

Materials and methods

Reagents and chemicals

Pure C_{60} (99.5%) was produced from NeoTech Product Company, Russia and confirmed by thin-layer chromatography (TLC, SiO_2, toluene). Reagents of tris(dibenzylideneacetone)dipalladium(0), *rac*-2,2'-bis(diphenylphosphino)-1,1'-binaphthyl (BINAP), 2-bromofluorene, and all other chemicals were purchased from Sigma-Aldrich Chemicals.

Physical measurements for material characterization

Infrared spectra were recorded as KBr pellets on a Thermo Nicolet 370 series FT-IR spectrometer. UV-Vis spectra were recorded on a Perkin Elmer Lambda-9 UV/VIS/NIR spectrometer. ^{1}H NMR and ^{13}C NMR spectra in solution were taken on Bruker Avance Spectrospin-500 spectrometer. Fluorescence spectra were collected on a FLUOROLOG (ISA Instruments) spectrofluorometer. Mass spectroscopic measurements were performed by the use of positive ion matrix-assisted laser desorption ionization (MALDI–TOF) technique on a micromass M@LDI-LR mass spectrometer. In a typical measurement, two fractions (100 μl) each from the solution of C_{60}(>DPAF-C_9)$_x$ (1.0 mg) in chloroform (1.0 ml) and the matrix solution of α-cyano-4-hydroxycinnamic acid (10 mg) in acetone (1.0 ml) were mixed together. From this sample-matrix mixture, a small quantity (2.0 μl) was taken and deposited on the stainless steel sample target plate, dried, and, subsequently, inserted into the ionization source of the instrument. The resulting sample blended or dissolved in the matrix material was irradiated by nitrogen UV laser at 337 nm with 10 Hz pulses under high vacuum. MALDI mass spectra were acquired in reflectron mode. Each spectrum was produced by averaging 10 laser shots; at least 25 spectra were acquired from different regions of the sample target. Mass ion peaks were identified for the spectrum using the MassLynx v4.0 software.

Preparation of 7-α–bromoacetyl-9,9-di(3,5,5-trimethylhexyl)-2-diphenylaminofluorene (7)

A modified aluminum chloride quantity to the literature procedure was applied.[30,38] A solution of 9,9-di(3,5,5-trimethylhexyl)-2-diphenylaminofluorene **6** (1.4 g, 2.4 mmol) in 1,2-dichloroethane (30 ml). was added to a suspension of aluminum chloride (1.12 g, 8.4 mmol, 3.5 equiv.) in 1,2-dichloroethane (50 ml) at 0 ^{o}C. The mixture was then added by α-bromoacetyl bromide (0.25 ml, 6.5 mmol) dropwise over a period of 5.0 min while maintaining the reaction temperature between 0–10 ^{o}C. The mixture was slowly warmed to ambient temperature and stirred for an additional 8.0 h. At the end of the reaction, it was quenched by slow addition of ice cold water (100 ml) while maintaining the temperature below 45 ^{o}C. The organic layer was separated and washed sequentially with dil. HCl (1.0 N, 50 ml) and water (50 ml, twice). The liquid was dried over magnesium sulfate and concentrated in vacuo to obtain the crude

product as crystalline yellow solids. Further purification was made by column chromatography (silica gel) using a mixture of hexane–EtOAc (9:1) as the eluent. A chromatographic fraction corresponding to R_f = 0.6 on TLC (SiO_2, hexane:EtOAc/9:1 as the eluent) was isolated to afford 7-α–bromoacetyl-9,9-di(3,5,5-trimethylhexyl)-2-diphenylaminofluorene **7** as yellow viscous oil in 68% yield (1.2 g). The spectroscopic characteristics of **7** were identical to those data reported.[29]

Synthesis of the [60]fullerenyl monoadduct 7-(1,2-dihydro-1,2-methanofullerene[60]-61-carbonyl)-9,9-di(3,5,5-trimethylhexyl)-2-diphenylaminofluorene, **C_{60}(>DPAF-C_9) 1**, **and the corresponding bisadduct C_{60}[methanocarbonyl-7-(9,9-di(3,5,5-trimethylhexyl)-2-diphenylaminofluorene)]$_2$, C_{60}(>DPAF-C_9)$_2$ 2**

A modified reagent quantity to the literature procedure was applied.[30] C_{60} (700 mg, 0.97 mmol) dissolved in toluene (600 ml) was added 7-α-bromoacetyl-9,9-di(3,5,5-trimethylhexyl)-2-diphenylaminofluorene **7** (686 mg, 0.97 mmol, 1.0 equiv.) under an atmospheric pressure of nitrogen. To this solution was added 1,8-diazabicyclo[5.4.0]undec-7-ene (DBU, 0.18 ml, 1.16 mmol) and stirred at room temperature for a period of 5.0 h. At the end of stirring, suspending solids of the reaction mixture were filtered off, washed with toluene, and the filtrate was concentrated to a 10% volume. Methanol (100 ml) was then added to cause precipitation of the crude product, which was isolated by centrifugation. Analytical thin-layer chromatography (TLC, SiO_2) of the solid sample indicated a mixture of several products at different R_f values. Only two major narrow bands were isolated by column chromatographic separation on silica gel using a solvent mixture of hexane–toluene (1:2) as the eluent. The first chromatographic band, corresponding to a spot at R_f = 0.85 on the analytical TLC plate using a mixture of hexane–toluene (2:3) as the eluent, afforded the monoadduct 7-(1,2-dihydro-1,2-methanofullerene[60]-61-carbonyl)-9,9-di(3,5,5-trimethylhexyl)-2-diphenylamino-fluorene, C_{60}(>DPAF-C_9) **1**, as brown solids (680 mg, 68% based on recovered C_{60} in 135 mg quantity). Spectroscopic data of **1**: MALDI–MS (TOF) calcd for $^{12}C_{105}{}^{1}H_{55}{}^{14}N^{16}O$ *m/z* 1345.4; found, *m/z* 1349, 1348, 1347, 1346 (MH^+), 894, 877, 862, 855, 845, 840, 802, 704, 687, 683, 672, 665, 650, 631, 629, 612, and 585; FT-IR (KBr) υ_{max} 3435 (br), 2947 (s), 2922, 2861 (m), 1678, 1593 (vs), 1491 (s), 1464, 1426, 1402, 1347 (w), 1274 (s), 1199 (s), 1185, 1155 (w), 1028 (w), 816 (w), 752 (s), 695 (s), 576, and 526 (vs) cm^{-1}; ^{1}H NMR (500 MHz, $CDCl_3$, ppm) δ 8.47 (d, J = 8.0 Hz, 1H), 8.33 (s, 1H), 7.82 (d, J = 8.0 Hz, 1H), 7.65 (d, J = 8.0 Hz, 1H), 7.26 (m, 6H), 7.13 (m, 4H), 7.05 (m, 2H), 5.67 (t, J = 4.0 Hz, 1H), 2.1–1.9 (m, 4H), 1.3–1.1 (m, 4H), and 0.9–0.6 (m, 30H).

The second chromatographic band, corresponding to a spot at R_f = 0.73 on the analytical TLC plate using a solvent mixture of hexane–toluene (2:3) as the eluent, gave the bisadduct

C_{60}(methanocarbonyl-9,9-di(3,5,5-trimethylhexyl)-2-diphenylaminofluorene)$_2$, C_{60}(>DPAF-C_9)$_2$ **2**, as brownish solids in 9% yield (130 mg). Spectroscopic data of **2**: MALDI–MS (TOF) calcd for $^{12}C_{150}{}^{1}H_{110}{}^{14}N_2{}^{16}O_2$ *m/z* 1970.8; found, *m/z* 1974, 1973, 1972, 1971 (M^+), 1347, 1346, 870, 861, 710, 705, 672, 666, 630, 629, 612, and 583; FT-IR (KBr) υ_{max} 3429 (br), 3163, 2951 (s), 2922, 2863, 1680, 1595 (vs), 1492 (vs), 1465, 1420, 1400, 1316(w), 1277, 1200, 1156 (w), 1093, 1030 (w), 816 (w), 753, 670 (s), and 527 cm^{-1}; ^1H NMR (500 MHz, $CDCl_3$, ppm) δ8.5–8.1 (m, 4H), 7.9–7.4 (m, 4H), 7.24 (m, 12H), 7.12 (m, 8H), 7.05 (m, 4H), 5.8–5.3 (m, 2H), 2.1–1.8 (m, 8H), 1.35–1.15 (m, 8H), and 1.1–0.5 (m, 60H).

Synthesis of the [60]fullerenyl tetraadduct C_{60}[methanocarbonyl-7-(9,9-di(3,5,5-trimethylhexyl)-2-diphenylaminofluorene)]$_4$, C_{60}(>DPAF-C_9)$_4$ 3a and 3b

Finely divided C_{60} (550 mg, 0.76 mmol), 7-α-bromoacetyl-(9,9-di(3,5,5-trimethylhexyl)-2-diphenylaminofluorene (3.24 g, 4.6 mmol, 6.0 equiv.), and anhydrous toluene (500 ml) were placed in a reaction flask under nitrogen atmosphere. The mixture was stirred at ambient temperature until a clear solution was obtained. To this solution was added 1,8-diazabicyclo[5.4.0]undec-7ene (DBU, 850 mg, 5.5 mmol, 7.2 equiv.). The reaction mixture was stirred at room temperature for a period of 8.0 h to result in a fine-solid suspended solution. Solid particles in the solution were filtered and washed with toluene. The combined filtrate was concentrated to 50 ml. To this concentrated liquid was added methanol (100 ml) to effect precipitation of the crude products, which were isolated by centrifugation. The crude solids were washed with methanol (3 × 20 ml) and subsequently purified by column chromatography (silica gel) using a solvent mixture of hexane–toluene (3:1) as the eluent. Prior to column chromatography, the crude sample was evaluated on analytical TLC plates to observe at least 4 product spots each in a different relative quantity. However, only two major fractions were collected by column chromatography separation and subsequently repurified separatedly on preparative TLC plates [SiO_2, 2,000 μm layer thickness, using a solvent mixture of hexane–toluene (4:1) for the less polar fraction and hexane–toluene (3:1) for the more polar fraction as the eluent]. During the TLC separation, only a center narrow dense band was isolated to afford the [60]fullerenyl multiadducts. These two product fractions were identified to be the tetraadducts; C_{60}[methanocarbonyl-7-(9,9-di(3,5,5-trimethylhexyl)- 2-diphenylaminofluorene)]$_4$ **3a**, corresponding to the chromatographic band at R_f= 0.5 on analytical TLC plate using hexane–toluene (2:3) as the eluent, as brownish solids in 18% yield (440 mg) and **3b**, corresponding to the chromatographic band at R_f= 0.25 on analytical TLC plate, as brownish solids in 7% yield (170 mg). All other unidentified minor products from column chromatography were accounted for a total 470 mg.

Spectroscopic data of the nonpolar tetraadduct **3a**: MALDI–MS (TOF) calcd for $^{12}C_{240}{}^{1}H_{220}{}^{14}N_4{}^{16}O_4$ *m/z* 3221.6; found, *m/z* 3228, 3227, 3226, 3225, 3224, 3223, 3222 (M^+), 2639, 2619, 2560, 2599, 2597, 2540, 2127, 2104, 2102, 1972, 1563, 1547, 1543, 1479, 1468, 1456, 1347, 878, 870, 857, 827, 629, 612, and 531; FT-IR (KBr) υ_{max} 3421 (br), 2952 (vs), 2924 (vs), 2866, 1681, 1595 (vs), 1493 (vs), 1465, 1421, 1377 (w), 1347 (w), 1277, 1200, 1156 (w), 1029, 819, 752, 697 (s), 525, and 475 cm^{-1}; ^1H NMR (500 MHz, $CDCl_3$, ppm) δ 8.5–8.0 (m, 8H), 7.9–7.5 (m, 8H), 7.24 (m, 20H), 7.1–6.9 (m, 28H), , 5.6–5.0 (m, 4H), 2.4–1.7 (m, 16H), 1.4–1.1 (m, 16H), and 1.1–0.5 (m, 120H).

Spectroscopic data of the polar tetraadduct **3b**: MALDI–MS (TOF) calcd for $^{12}C_{240}{}^{1}H_{220}{}^{14}N_4{}^{16}O_4$ *m/z* 3221.6; found, *m/z* 3228, 3227, 3226, 3225, 3224, 3223, 3222 (M^+), 2785, 2770, 2757, 2755, 2754, 2753, 2731, 2730, 2680, 2658, 2622, 2599, 2145, 2130, 2128, 2106, 2105, 2104, 1974, 1972, 1958, 1067, 1003, 948, 947, 946, 827, 629, 612, and 531; FT-IR (KBr) υ_{max} 3434 (br), 2951 (s), 2924 (vs), 2864, 1683, 1594 (vs), 1492 (vs), 1466, 1420 (w), 1363 (w), 1316 (w), 1278, 1211, 1177 (w), 1089, 819, 752, 697 (s), 525, and 474 (br) cm^{-1}; ^1H NMR (500 MHz, $CDCl_3$, ppm) δ 8.6–8.1 (m, 8H), 7.9–7.5 (m, 8H), 7.24 (m, 20H), 7.11(m, 20H), 7.03 (m, 8H), 5.6–4.9 (m, 4H), 2.2–1.8 (m, 16H), 1.4–1.1 (m, 16H), and 1.1–0.4 (m, 120H).

Optical absorption measurements

Optical absorption and transmission spectra, in the range of 180–1200 nm, of C_{60}(>DPAF-C_9)$_x$ (x = 1, 2, or 4) samples dissolved in CS_2 were determined in a 1-mm-thick quartz cuvette with a UV-Vis-NIR spectrophotometer (Model UV 3600, Shimadzu, Kyoto, Japan).

Two-photon absorption cross-section (σ_2) and nonlinear optical transmittance measurements

Two-photon absorption cross-section (σ_2) and nonlinear optical transmittance measurements of C_{60}(>DPAF-C_9)$_x$ (where x = 1, 2, or 4) samples in a CS_2 solution were carried out with femtosecond Z-scans and energy-dependent transmission counting at the wavelength of 780 nm. To reduce accumulative thermal effects and to minimize the contribution of triplet-triplet state absorption in C_{60}(>DPAF-C_9)$_x$, we employed 150-fs laser pulses at 1-kHz repetition rate. Laser pulses were generated by a mode-locked Ti:Sapphire laser (Quantronix, IMRA), which seeded a Ti: Sapphire regenerative amplifier (Quantronix, Titan), and focused onto a 1-mm-thick quartz cuvette containing a solution of C_{60}(>DPAF-C_9)$_x$ with a minimum beam waist of ~12 μm. By adding CS_2 to C_{60}(>DPAF-C_9)$_x$, concentration of the samples was adjusted to either 1.0×10^{-4}, 1.86×10^{-3}, or 1.0×10^{-2} M for the measurement. Incident and transmitted laser powers were monitored as the cuvette was moved (or Z-scanned) along the propagation direction of laser pulses.

Two-photon absorption is described by the change in the absorption coefficient $\Delta\alpha = \beta I$, where β and I are the 2PA coefficient and the light intensity, respectively. The 2PA coefficient can be extracted from the best fitting between the Z-scan theory[39] and the data. The 2PA cross-section value was then calculated from the 2PA coefficient by the formula $\sigma_2 = \beta\hbar\omega/N$, where $\hbar\omega$ is the photon energy and N is the number of the molecules.

Results and discussion

The compounds of 9,9-dialkyldiphenylaminofluorenes (DPAF-C_n) are electron donors (D) and highly fluorescent materials showing emission at ~450 nm upon photoexcitation at <400 nm. Its conjugation with the C_{60} acceptor (A) cage facilitates intramolecular electron- and energy-transfer events from DPAF moiety to fullerene moiety in C_{60}–DPAF assemblies in an ultrafast kinetic rate of >10 ps after a 150-fs laser irradiation.[31] In a nonpolar solvent, such as toluene, triplet state of the fullerene cage in $^3C_{60}$*(>DPAF-C_2) has a lifetime of 33 μs.[31] As we extended this linear D-A arrangement to include multiple DPAF-C_n attachments on one C_{60} cage, corresponding starburst A-$(D)_n$ or C_{60}-$(DPAF\text{-}C_n)_x$ structures were formulated. In this structural motif, the C_{60} cage becomes a molecular core and multiple DPAF-C_n subunits are photoactive antenna components to harvest light from visible (for single photon excitation) to near infrared (for two-photon excitation) wavelength ranges. Subsequent transfer of the excited-state energy to the central fullerene core may enhance its reverse saturable absorption capability. In a very dilute solution giving a nearly molecularly separated state of each C_{60}-$(DPAF\text{-}C_n)_x$, interference of intermolecular energy transfer and excited state quenching may be minimized. As their concentration increases in the materials application, molecular aggregation and coalescence becomes a common phenomenon that may significantly affect the photoresponsive efficiency of the compound. One approach to extend and maintain the molecular photoefficiency in highly concentrated solution or solid state is to apply highly bulky groups in the structure as a physical barrier to favor molecular separation. One recent example was given by hindered C_{60}(>DPAF-C_9) and C_{60}(>DPAF-C_9)$_2$, where C_9 is denoted as 3,5,5-trimethylhexyl group, showing enhanced 2PA cross-section values and nonlinear optical responses.[28] Reduction in some extent of molecular aggregation in a dense solution without much decrease of the chromophore density is reasoned for this enhancement.

Cluster formation of fullerenes in solution can be frequent occurrence during the sample preparation owing to a strong tendency of hydrophobic attraction among fullerene cages via weak intermolecular van der Waals interactions in nonpolar solvents, such as benzene, toluene, and CS_2.[40,41] Evidently, the phenomenon exists even in fairly dilute toluene solution in a concentration of 2×10^{-4} M showing fractal clusters $(C_{60})_n$ ($n \geq 3$) with sizes >1.2 nm other than single C_{60} molecules.[42] Quantum efficiency of the

triplet population can be considerably depleted in the form of particles and clusters, via triplet-triplet annihilation.

In the presence of an extended aromatic DPAF ring in C_{60}(>DPAF-C_2) structure, strong fullerenyl π-interactions were found to drive the molecular assembly over DPAF-C_2 subunits into a highly ordered array of the fullerene cages in its single crystal structure.[30] The structural arrangement also forces planar DPAF-C_2 rings to orient side-by-side to each other with no direct π-π interaction between DPAF moieties, indicating stronger interactions among C_{60} cages than DPAFs or between C_{60} and DPAF. Therefore, it may require at least four DPAF-C_n subunits, such as in C_{60}(>DPAF-C_9)$_4$, to encapsulate the C_{60} cage in addition to the attachment of hindered 3,5,5-trimethylhexyl groups on C_9 position of the fluorene ring to prevent direct intermolecular stacking contact of both fullerene cages and DPAF-C_n rings. In addition, when C_{60} cages are wrapped by four hindered dialkylated chromophores, enhanced solubility of the resulting macromolecule should lead to a larger amount of C_{60} cages being drawn into the solvent for a highly concentrated solution.

Synthesis and structural characterization of C_{60}-DPAF conjugates

Preparation of the dyad C_{60}(>DPAF-C_9) **1**, 7-(1,2-dihydro-1,2-methanofullerene[60]-61-carbonyl)-9,9-di(3,5,5-trimethylhexyl)-2-diphenylaminofluorene, and the triad C_{60}(>DPAF-C_9)$_2$ **2**, C_{60}[methanocarbonyl-7-(9,9-di(3,5,5-trimethylhexyl)-2-diphenylaminofluorene)]$_2$, followed a modified synthetic procedure reported recently.[30] The modification included the use of a larger quantity of aluminum chloride (3.5 equiv.) in Friedel-Crafts acylation reaction with α-bromoacetyl bromide than the reported amount to obtain a good product yield of 7-α–bromoacetyl-9,9-di(3,5,5-trimethylhexyl)-2-diphenylaminofluorene **7**. Isolation and purification of **2** were made by the collection of only a narrow, major chromatographic band on preparative TLC plates corresponding to a spot at R_f = 0.73 on the analytical TLC plate using a solvent mixture of hexane–toluene (2:3) as the eluent. Synthesis of starburst C_{60}-DPAF conjugates was carried out by using multiple equivalents of α–bromo-DPAF-C_9 **7** per C_{60} under similar reaction conditions. However, a greater quantity of **7** than 2.0 equiv. used in the reaction resulted in a distribution of bisadducts, trisadducts, and tetraadducts along with other minor higher multiadducts with little control. Therefore, we applied a maximum quantity of **7** in 6.0 equiv. for this reaction by considering the bulky size of DPAF-C_9 with a sufficient reaction time to complete the highest possible number of chromophore attachments on each C_{60}. The approach minimizes the products containing lower numbers of DPAF-C_9 arms and maximizes the product yield of high multiadducts that simplifies the product separation. Evidently, at least 4 chromatographic spots were clearly visible on analytical TLC plates each in a different relative quantity. Among them, only two major fractions were collected by column chromatographic separation and subsequently repurified individually as a narrow

band on preparative TLC plates (SiO_2) to afford the major multiadduct products identified later to be [60]fullerene pentad isomers. No significant quantity of [60]fullerene hexaads or higher adducts were isolable. The first fraction of these two products, corresponding to the chromatographic band at R_f = 0.5 on analytical TLC plate using hexane–toluene (2:3) as the eluent, is less polar. It was found to be the tetraadduct C_{60}(>DPAF-C_9)$_4$, C_{60}[methanocarbonyl-7-(9,9-di(3,5,5-trimethylhexyl)-2-diphenylaminofluorene)]$_4$ **3a**, in the form of brownish solids in 18% yield. The next major polar fraction, corresponding to the chromatographic band at R_f = 0.25 on analytical TLC plate, was the second tetraadduct **3b** isolated as brownish solids in 7% yield. All other product fractions in a combined quantity were accounted for another roughly 20% yield of minor, unidentified tetraads, pentaads, or hexaads.

Chemical structures of **1** and its related monoadduct C_{60}(>DPAF-C_2) were well characterized by spectroscopic methods with the latter also by x-ray single crystal structural analyses.[30] Their spectroscopic data greatly aided the structural correlation, characterization, and identification of **2**, **3a**, and **3b** in this report. Monofunctionalization of C_{60} occurs only on one-half of the sphere leaving the other half-sphere remaining intact. Accordingly, infrared spectrum of **1** (Fig. 1b) showed two sharp characteristic bands at 576 and 526 cm^{-1} in nearly identical peak positions to those of pristine C_{60} (Fig. 1a) at 575 and 526 cm^{-1}, respectively. Therefore, these two sharp bands are characteristically useful as the structural indicator for the bisadducts and tetraadducts if all functional groups are attached on C_{60} at the same half-sphere. In comparison with the molecular diameter of C_{60}, the size of the moiety 7-keto-9,9-di(3,5,5-trimethylhexyl)-2-diphenylaminofluorene (DPAF-C_9, Scheme 1) is relative bulky that can be considered as a hindered arm. It is plausible to assume that the attachment of two DPAF-C_9 arms on one C_{60} should result in regioisomers each with two DPAF-C_9 subunits located in a separation distance enough to accommodate the gyration radius of these chromophore arms. Large reduction in intensity of two sharp bands at 576 and 526 cm^{-1} in the infrared spectrum (Fig. 1c) of the triad C_{60}(>DPAF-C_9)$_2$ revealed only a minor quantity of a regioisomer with two DPAF-C_9 subunits located on the same half-sphere in the isolated major chromatographic band. These two sharp bands disappeared fully in the infrared spectra (Figs. 1d and 1e) of the pentaad isomers C_{60}(>DPAF-C_9)$_4$ **3a** and **3b**, indicating a distribution of four bulky DPAF-C_9 subunits around the full sphere of C_{60}. Undoubtedly, IR spectra of all C_{60}-DPAF conjugates **1**, **2**, **3a**, and **3b** displayed a nearly identical profile of the bands corresponding to optical absorption of DPAF-C_9 moiety. It included the characteristic band centered at 1683 cm^{-1}, corresponding to absorption of a keto group bridging a methano[60]fullerene (C_{60}>) cage and a fluorene moiety, in a roughly 50 cm^{-1} shift from the normal carbonyl stretching band at 1720–1750 cm^{-1} due to influence of the fluorene ring structure.

Molecular weight of the triad **2** was clearly confirmed by positive ion matrix-assisted laser desorption ionization mass spectrum (MALDI–MS), using α-cyano-4-hydroxycinnamic acid as the matrix, displaying a group of mass peaks with a maximum peak intensity centered at *m/z* 1972, as shown in Fig. 2. Analysis of this group in Fig. 2b indicated the molecular ion mass (M^+) of **2** at *m/z* 1971 with following protonated MH^+ and isotope peaks at *m/z* 1972–1974. It was followed by a group of mass peaks centered at *m/z* 1346 matching well with that of the monoadduct **1** resulting from the loss of exact one CH_2(DPAF-C_9) (*m/z* 626) subunit from the molecular mass. In the low mass ion region, several major peaks at *m/z* 612–629 corresponding to the mass of DPAF-C_9 (*m/z* 612) and CH(DPAF-C_9) (*m/z* 625) were also observed revealing facile fragmentation at the bonds immediately next to the C_{60} and methano[60]fullerene cage. The relatively simple spectrum in the high mass region revealed good stability of aromatic *keto*-diphenylaminofluorene moiety under MALDI–MS measurement conditions.

In the MALDI–MS investigation of the tetraadducts **3a** and **3b**, a significantly higher laser power than that used in the measurement of **2** was necessary to overcome the low intensity of the mass ion above *m/z* 3000. However, application of a high laser power created additional mass ion peaks as spectral contaminant with one or two carbon mass units (*m/z* 15, 24, or higher, *etc*.) higher than the molecular ion or fragmented ion masses. In the high mass region, a group of sharp mass ion peaks corresponding to the molecular mass of C_{60}(>DPAF-C_9)$_4$ **3a** at *m/z* 3222 (M^+) and its isotope peaks at *m/z* 3222–3228 were detected, as shown in Fig. 3. Two additional groups of higher mass ions at *m/z* 3247 $(M + 24)^+$ and 3263 were, presumably, the result of high laser power conditions. The next major group of mass fragmentation peaks occurring at *m/z* 2599 (Fig. 3a) matched well with the mass of protonated C_{60}(>DPAF-C_9)$_3$ by the loss of one CH(DPAF-C_9) group (*m/z* 625) from **3a**. Further fragmentation of C_{60}(>DPAF-C_9)$_3$ mass peak to give the corresponding C_{60}(>DPAF-C_9)$_2$ and C_{60}(>DPAF-C_9) mass ions at *m/z* 1972 and 1347, respectively, was also observed in a relatively low intensity. In the low mass ion region, two sharp peaks at *m/z* 612 and 629 corresponding to the mass of DPAF-C_9 and CH_x(DPAF-C_9), respectively, was detected in a high peak intensity, implying fast loss of two CH(DPAF-C_9) groups after the C_{60}(>DPAF-C_9)$_3$ fragment. These mass spectrum data evidently substantiated the mass composition of **3a** as C_{60}(>DPAF-C_9)$_4$. The mass ion peak at *m/z* 2104 was the result of decarboxylation fragmentation of C_{60}(>DPAF-C_9)$_2$-(α-cyano-4-hydroxycinnamic acid) adduct generated under high voltage MALDI–MS conditions.

Comparison of ^{1}H NMR spectra among **1**, **2**, **3a**, and **3b** was made in Fig. 4, where chemical shift values of all protons of C_{60}(>DPAF-C_9) were used as the reference for the proton assignment of the bisadducts and tetraadducts. Interestingly, the α-proton (H_α, next to the carbonyl group) peak of **1**

appeared as a triplet-like signal, perhaps due to long-range $^1H–^1H$ coupling, at δ 5.67 (Fig. 4a) with a large downfield shift of 1.15 ppm from that of **7** (δ 4.52, singlet). It was accompanied with three groups of phenyl proton peaks of H_5, H_6, and H_8 of DPAF moiety showing corresponding chemical shifts at 7.82 (d, J = 8 Hz), 8.46 (d, J = 8 Hz) and 8.33 (s), respectively. Benzyl proton (H_9) peaks at δ 1.9–2.1 are apparently indicative of non-equal H_9s showing two groups of multiplet, instead of one triplet, signals. Peak splitting of benzyl protons is caused by steric hindrance of adjacent bulky diphenylamino group. In the case of C_{60}(>DPAF-C_9)$_2$, a comparable ^1H NMR spectrum (Fig. 4b) to that of Fig. 4a was obtained. Accordingly, we assigned multiplet peaks at δ 8.1–8.5 (4H), 7.63–7.8 (2H), 5.3–5.8 (2H), and 1.8–2.1 (8H) for the chemical shift of H_6–H_8/$H_{6'}$–$H_{8'}$, H_5/$H_{5'}$, H_a/H_b, and H_9s protons, respectively, of **2**. Considering two possible sterically non-equivalent CH(DPAF-C_9) subunits and the peak splitting pattern of H_6, H_5, H_a, and H_9 as the reference, the profile of α-proton peak in the region of δ 5.3–5.8 was separated into two groups at δ 5.3–5.55 and 5.55–5.8 with a proton integration ratio of roughly 2.5:1. That revealed the same molecular ratio of two possible regioisomers of C_{60}(>DPAF-C_9)$_2$ in a similar molecular polarity. By applying the analyses made on its IR spectrum, the minor regioisomer might contain two CH(DPAF-C_9) arms on the same half-sphere, whereas the major regioisomer might contain two CH(DPAF-C_9) arms located on the opposite half-sphere to each other. As the spectrum extended to those of C_{60}(>DPAF-C_9)$_4$ **3a** and **3b**, as shown in Figs. 4c and 4d, a slight upfield shift of α-proton multiplet to δ 4.9–5.6 with increasing complexity was detected. In principle, a high number of four DPAF-C_9 addends per C_{60} as in **3a** and **3b**, giving a close resemblance to molecular encapsulation of C_{60}, should increase significantly the spatial crowdedness surrounding the fullerene cage and decrease the degree of freedom for each DPAF-C_9 arm to make free-rotation around C_{61}–(C=O) bond. That reduces the peak resolution of α-protons H_a, H_b, H_c, and H_d of **3** and, thus, broadens further their peak profiles. Therefore, based on the peak profiles of H_6/$H_{6'}$/$H_{6''}$/$H_{6'''}$, H_8/$H_{8'}$/$H_{8''}$/$H_{8'''}$, and H_5/$H_{5'}$/$H_{5''}$/$H_{5'''}$ of **3a** (Fig. 4c) and **3b** (Fig. 4d) at δ 7.65–8.5, both with reasonably close similarity in peak resolution and shape to those of **2** (Fig. 4b) in the same chemical shift region allowed us to suggest a low possible number of non-isolable regioisomers, such as that of **2**, in the narrow chromatographic fractions of **3a** and **3b**.

Relative integration ratio of aromatic proton peaks at δ 7.0–8.6 of ^1H NMR spectra of C_{60}(>DPAF-C_9), C_{60}(>DPAF-C_9)$_2$, and C_{60}(>DPAF-C_9)$_4$ can be used as the value for quantitative counting of the total aromatic protons that, in term, correlate directly to the number of DPAF-C_9 units per molecule. The compound 1,4-diazabicyclo[2.2.2]octane (DABCO) is a symmetrical molecule showing only one singlet ^1H peak at δ 2.78 for 12 protons in a chemical shift region containing no aliphatic proton peaks of DPAF-C_9 moiety. Therefore, this proton peak taken in a known applied

concentration can be used as the internal standard for the proton counting among the peaks shown in ^{1}H NMR spectra of Figs. 4a–4d. The procedure of relative integration ratio measurements and the calculation were given as a part of the supporting data. Consequently, the results showed a total number of aromatic protons of **1** (Fig. 4a), **2** (Fig. 4b), and **3** (Figs. 4c and 4d) in good agreement with the corresponding chemical structure containing one, two, and four DPAF addends, respectively, per C_{60} cage. The data provided further confirmation of the structural composition of these compounds.

Two-photon absorption cross-section (σ_2) measurements of C_{60}-DPAF conjugates at a high laser power

Two-photon absorption (2PA) cross section values of two C_{60}-DPAF conjugates C_{60}(>DPAF-C_9) and C_{60}(>DPAF-C_9)$_2$ measured in both femtosecond and nanosecond regions using the a low laser power of 10–30 GW/cm^2 were reported recently.[28] In the present study, 2PA properties of C_{60}(>DPAF-C_9)$_x$ (where x = 1, 2, and 4) dissolved in CS_2 were investigated with femtosecond *Z*-scans measurements at 780 nm. To correlate the 2PA data with the results of energy-dependent nonlinear transmission study, a relatively high energy power source at 163 GW/cm^2 (or 24.5 mJ/cm^2) was applied. This power intensity range also facilitates the signal detection on the same sample in a low solution concentration down to 1.0×10^{-4} M. However, high laser-pulse irradiation to fullerene solutions has been reported to cause thermally induced scattering effects.[11,43] For preventing much deviation of measured 2PA cross-section values from intrinsic two-photon absorptions, effort was taken to reduce accumulative thermal effects to a possibly low level and to minimize the contribution of triplet-triplet state absorption in these fullerenyl chromophores by employing ultrafast 150-fs laser pulses at 1-kHz repetition rate. Nevertheless, it cannot rule out completely the contribution of thermally induced scattering effect to result in somewhat larger 2PA cross sections measured. By assuming this thermal effect to the scattering being similar on all C_{60}(>DPAF-C_9)$_x$ solutions, the 2PA data should be qualitatively useful for comparison analyses. Prior to 2PA measurements, the concentration of all C_{60}(>DPAF-C_9)$_x$ solution in CS_2 was adjusted to 1.86×10^{-3} M that gives a linear (or low-fluence) transmittance (*T*) of 88.6% in a nearly identical intensity for all samples at 780 nm, as shown in Fig. 5. As the concentration was increased to 1.0×10^{-2} M, the solution transmittance of **1**, **2**, **3a**, and **3b** decreased to a slightly different level of 77, 82, 80, and 82%, respectively, at 780 nm. Among them, a relatively small deviation of transmittance intensity for the monoadduct C_{60}(>DPAF-C_9) solution might be attributed to its higher tendency to aggregate in a high concentration than the rest of multiadducts. Molecular aggregation of **1** and **2** was expected to result in broadening and the shift of their optical absorption bands from the maxima at 326 (for fullerene cage) and 410 (for DPAF moiety) nm to a slightly longer wavelength along with a shift of the transmission edge from roughly 570 to 680 nm.

Both C_{60} and diphenylaminofluorene components are photoresponsive chromophores capable of undergoing simultaneous two-photon excitation, making contributions to the two-photon absorption cross-section value. To differentiate the molecular contribution vs. the number-sum component contribution to measured 2PA cross-section values (σ_2) and gain an insight of structure–property relationship leading to the enhancement of σ_2, we carried out comparative *Z*-scans (Fig. 6) to include measurements based on the cumulative number-sum of individual C_{60} and CH_3(DPAF-C_9) components in the same composition ratio as that of their corresponding conjugated compounds C_{60}(>DPAF-C_9)$_x$. For the comparison purpose, it was performed in CS_2 with the concentration of 1.0×10^{-4} M. As a result, a systematic increase of σ_2 value from 12.7×10^{-48} cm^4.sec.photon^{-1}.molecule^{-1} for the combination of one C_{60} and one CH_3(DPAF-C_9) model component to 29.6 and 46.4×10^{-48} cm^4.sec.photon^{-1}.molecule^{-1} for the combination of one C_{60} with two and four CH_3(DPAF-C_9) components, respectively, was observed, as shown in Table 1. At a relatively low concentration of 1.0×10^{-4} M, an unimolecular process of either C_{60} or CH_3(DPAF-C_9) model component in response to laser excitation may be expected. Based on this assumption and the simple cumulative sum of 2PA data measured, the average 2PA contribution of one molecular fraction of CH_3(DPAF-C_9) component to the σ_2 value can be estimated to be roughly $11–12 \times 10^{-48}$ cm^4.sec.photon^{-1}.molecule^{-1}. That implied DPAF-C_9 being the major structural moiety in C_{60}(>DPAF-C_9)$_x$ responsible for photoexcitation in 2PA processes at 780 nm. The implication is reasonable since we believe the 2PA peak of structurally modified C_{60} is to be at the wevelengths >950 nm.[24]

Similar open-aperture *Z*-scans carried out under the irradiance of 163 GW/cm^2 were taken for **1**, **2**, **3a**, and **3b** in CS_2 in three concentrations from 1.0×10^{-4} to 1.0×10^{-2} M with the plots shown in Fig. 7. These *Z*-scans displayed positive signs for absorptive nonlinearities. All calculated values of 2PA coefficient β and cross sections σ_2 of these chromophores are listed in Table 1, where nonlinear absorption in neat carbon disulfide was also measured and included as the reference that gave the β value of 0.03 cm/GW in a similar range of the value (0.05 cm/GW) reported recently.[44] As thermally induced scattering effects caused by high irradiances may influence the accuracy of overall 2PA cross sections measured, we undertook the measurement of *Z*-scans of C_{60}(>DPAF-C_9)$_4$ **3a** in CS_2 (1.86×10^{-3} M) at different irradiances, as shown in Fig. 8a, with the resulting 2PA cross-section values plotted as a function of the laser power intensity in Fig. 8b. Interestingly, the σ_2 values apparently remain nearly constant in approximately a straight line across the irradiance range from 40 GW/cm^2 up to 600 GW/cm^2 without an obvious increase, confirming the independence of σ_2 values on the laser power intensity. It can be interpreted as the thermally induced scattering contribution being either fluctuation

insensitive or relatively constant over the irradiance range. Thus, the observed change ($\Delta\sigma_2$) in the nonlinear absorption could be purely due to the difference of 2PA processes.

In the comparison of σ_2 values among C_{60}(>DPAF-C_9)$_x$ samples collected in 1.0×10^{-4} M concentration, a consistent reduction of the transmittance in Figs. 7a–7d were indicative of a larger 2PA coefficient of each C_{60}(>DPAF-C_9)$_x$ compound than that for the sum of compositional model components. Accordingly, an increase of 2PA cross sections in 2.0, 1.6, 1.9, and 1.4 folds of their corresponding model component σ_2 values for **1**, **2**, **3a**, and **3b**, respectively, revealed clearly the contribution of extending molecular branching and π-conjugative polarization of donor-acceptor moieties to the 2PA enhancement over the simple cumulative number-sum effect.

Most importantly, we observed a significant, consistent large increase of 2PA cross sections of all C_{60}(>DPAF-C_9)$_x$ compounds upon decrease of the solution concentration from 1.0×10^{-2} to 1.0×10^{-4} M in CS_2. Since 2PA cross sections for **1** and **2** in 2.0 and 1.0×10^{-2} M in CS_2 were reported in a value of 0.306 and 0.824×10^{-48} cm^4.sec.photon^{-1}.molecule^{-1} (or 30.6 and 82.4 GM), respectively, using a lower laser energy source of 10–30 GW/cm^2,[28] these two values were used for the calibration by reducing the measured σ_2 value of **2** at 1.0×10^{-2} M to the same amount as the reported one. Correspondingly, all other σ_2 values measured were then deducted by the same quantity of 3.4×10^{-48} cm^4.sec.photon^{-1}.molecule^{-1}, which is accounted for the partial factor arising from the thermally induced scattering,[11,43] to the new $\sigma_{2,adj}$ values, as shown in Table 1. As an example for **1**, the $\sigma_{2,adj}$ values were adjusted to be 8.0 and 21.9×10^{-48} cm^4.sec.photon^{-1}.molecule^{-1} (or 800 and 2,190 GM) at the concentration of 1.86×10^{-3} and 1.0×10^{-4} M, respectively, showing a clear increase of 2PA cross sections upon decrease of the concentration. Systematic increase of the σ value as $\Delta\sigma_{2,adj}$ at incremental decreases of the concentration was calculated as listed in Table 1. Interestingly, regardless of the multiadduct structure, the $\Delta\sigma_{2,adj}$ values in the high concentration range (10^{-3}–10^{-2} M) were relatively close to each other in a narrow range of $7.7–9.9 \times 10^{-48}$ cm^4.sec.photon^{-1}.molecule^{-1}, revealing domination of the aggregation factor over the difference of the molecular structure. As the degree of molecular separation increases at a low concentration of 10^{-4} M, a clear leap of $\Delta\sigma_{2,adj}$ values from 13.9, 33.2, to 48.1 and 68.2×10^{-48} cm^4.sec.photon^{-1}.molecule^{-1} for the modification of starburst structures going from the monoadduct **1**, bisadducts **2**, to tetraadducts **3b** and **3a**, respectively, was realized. The observation implied the significance of branched fullerenyl multiadducts in enhancing the 2PA cross-sections at the laser power range related to the nonlinear power transmission application.

We interpret the concentration-dependent phenomena by the high tendency of fullerene-DPAF chromophores to form nano-aggregates, instead of molecular dispersion, in a concentration above 10^{-3} M.

Nano-aggregation might play a role in reducing 2PA quantum efficiency leading to the decrease of the σ_2 value. Starburst structure of C_{60}(>DPAF-C_9)$_4$ pentaad regioisomers **3a** and **3b** gave the largest σ_2 enhancement over C_{60}(>DPAF-C_9) dyad and C_{60}(>DPAF-C_9)$_2$ triad when molecular dispersion became possible in dilute solution.

Nonlinear optical transmittance measurements of C_{60}-DPAF conjugates

Nonlinear optical transmittance properties of C_{60}-DPAF conjugates C_{60}(>DPAF-C_9)$_x$ in CS_2 were investigated by energy-dependent transmission measurements at the wavelength of 780 nm using the same setup as that in 2PA measurements conducted by 150 fs laser pulses, except the sample being fixed at the focus area when the incident pulse power was varied. Technical details of the measurements were described elsewhere.[45,46] Nonlinear transmittance results for 1-mm-thick solutions of **1**, **2**, **3a**, and **3b** in CS_2 at a medium concentration of 1.86×10^{-3} M were illustrated in Fig. 10a. All the samples showed a linear transmission (T = 88.6%) with input intensity of up to 36 GW/cm^2, or fluence of 5.4 mJ/cm^2. When the incident intensity was increased above 36 GW/cm^2, the transmittance (%) began to deviate from the linear transmission line and decrease indicating the initiation of nonlinearity and the limiting effect. The transmitted fluence further departed from the linear line upon the increase in the incident fluence. A systematic trend showing higher efficiency in reducing optical transmittance with the increase of irradiance level up to <1,000 GW/cm^2 was observed for the starburst tetraadducts C_{60}(>DPAF-C_9)$_4$ than that for the bisadduct C_{60}(>DPAF-C_9)$_2$ and the monoadduct C_{60}(>DPAF-C_9). Improvement in lowering the transmittance can be correlated to a higher number of DPAF-C_9 subunits in the structure of **3** than **1** and **2**, consistent with the positive contribution of a starburst structure as **3** to a larger two-photon absorption, concluded by *Z*-scans in Fig. 7. This correlation was made on the assumption of a similar degree of nonlinear scattering among the solutions.

In the molecular system of C_{60}(>DPAF-C_n)$_x$, simultaneous absorption of two photons energy at 780 nm leads to fast release of the fluorescence emission of DPAF-C_n at roughly 450 nm, which can be utilized for subsequent photoexcitation of the C_{60} cage via intramolecular energy transfer. The kinetic rate of following intersystem crossing going from the excited singlet state of the fullerene cage moiety ($^1C_{60}$*>) to the corresponding triplet state ($^3C_{60}$*>) took place within a 1.4 ns time scale.[28] Therefore, triplet–triplet state related absorption processes in the $^3C_{60}$*> cage moiety can be neglected in this study since the current measurements were performed by using 150 fs laser pulses. Observed transmittance reduction behavior may be attributed predominantly to the high absorption cross-section of 2PA processes, mainly on DPAF-C_9 moieties, and the excited state absorption of the lowest excited singlet state $^1C_{60}$*>. Population of the latter $^1C_{60}$*> state can be highly enhanced by ultrafast intramolecular

energy transfer from the two-photon pumped excited singlet state of DPAF-C_9 moiety in $C_{60}(>^1$DPAF*-$C_9)$ to form $^1C_{60}$*(>DPAF-C_9), which occurs in a rate as fast as 130 fs[28] to 15 ps.[31]

Under the conditions of *Z*-scan experiments, C_{60}(>DPAF-$C_9)_4$ showed surprisingly good photostability, which was evaluated by comparing the absorption spectra before and after laser irradiation. The results showed no difference in the spectral profiles for all the samples used. Even though the laser power applied was relatively high, and possibly had reached above the decomposition threshold of the C_{60}-DPAF molecule, the application of ultrafast irradiation in a time scale of femtosecond did not seem to have accumulated sufficient energy to impact the chromophore sample with noticeable damage. To evaluate the recovery time of observed nonlinearities and to reveal the underlying mechanism, we conducted a degenerate pump-probe experiment with 150-fs, 780-nm laser pulses close to the 2PA peak position of C_{60}(>DPAF-C_9) and C_{60}(>DPAF-$C_9)_4$ **3a** in CS_2 solution. As shown in Fig. 10b, the maximum transmittance change ($-\Delta T/T$) in **3a** solution was found to be greater than that in the solution of **1**, indicating larger 2PA coefficients and σ_2 values of **3a** than those of **1**. Furthermore, the response time of **3a** was evaluated to be ~15 ps in a time scale necessary for intramolecular energy transfer from DPAF-C_9 moiety to methano[60]fullerene (C_{60}>) moiety. It should be pointed out that an oscillation in the relaxation time was present. The origin of this oscillation is unclear. It may be attributed to the interplay between the 2PA and energy transfer processes.

Conclusions

We demonstrated an approach toward the design of starburst C_{60}-*keto*-DPAF assemblies to extend and maintain the molecular photoefficiency in highly concentrated solution by applying a combination of a starburst macromolecular configuration with C_{60} as an encapsulated core and multiple bulky groups. The structure was made for the progressive increase of aggregation barrier and unimolecular character. Molecular compositions of the resulting C_{60}(>DPAF-$C_9)_2$ triad and C_{60}(>DPAF-$C_9)_4$ pentaads, isolated from major, narrow chromatographic fractions, were confirmed by the analyses of their positive-ion MALDI-TOF mass spectra, using α-cyano-4-hydroxycinnamic acid as the matrix, that showed a group of the corresponding molecular mass ion peaks at *m/z* 1972 and 3222, respectively. Both C_{60}(>DPAF-$C_9)_2$ **2** and C_{60}(>DPAF-$C_9)_4$ (**3a** and **3b**) exhibited nonlinear optical transmittance reduction responses in femtosecond region with a lower transmittance % value for the latter at the high laser power range above 80 GW/cm^2. It was attributed to larger fs 2PA cross-section values of C_{60}(>DPAF-$C_9)_4$ than **2** in the same concentration and correlated to a higher number of DPAF-C_9 subunits in the structure of **3**.

All 2PA cross-section values of **1**, **2**, and **3** were found to be larger than that obtained from a solution mixture of C_{60} and DPAF-C_9 in the same component quantity derived from the corresponding molecular composition. It was reasoned by an increasing degree of intramolecular interaction and

polarization. As the concentration of the solution was varied systematically to induce molecular separation, a consistently large increase of 2PA cross sections of all C_{60}(>DPAF-C_9)$_x$ (x = 1, 2, or 4) chromophores in fs region was observed upon the concentration dilution from 1.0×10^{-2} to 1.0×10^{-4} M in CS_2. Difference of the 2PA cross section value change ($\Delta\sigma_2$) among all samples in response to variation of the concentration was not sensitive to the compound structure in the high concentration range. However, in a low concentration of 10^{-4} M, $\Delta\sigma_2$ values were evaluated to increase clearly from 13.9, 33.2, to 48.1 and 68.2 $\times 10^{-48}$ cm^4.sec.photon^{-1}.molecule^{-1} for the structural modification from the monoadduct **1**, bisadducts **2**, to tetraadducts **3b** and **3a**, respectively. This large $\Delta\sigma_2$ value enhancement for **3b** and **3a** was correlated to hindered starburst structures that may give a higher degree of molecular separation than **1** and **2** at a low concentration. Therefore, we interpreted the concentration-dependent phenomena by the high tendency of fullerene-DPAF chromophores to form nano-aggregates in a concentration above 10^{-3} M. In fact, nano-aggregation might play a role in reducing 2PA quantum efficiency leading to decrease of the σ_2 value. Starburst structure of C_{60}(>DPAF-C_9)$_4$ in a multipolar arrangement resembling encapsulation of C_{60} by multiple DPAF-C_9 chromophores is likely to increase the degree of molecular dispersion in a high solution concentration and hamper the aggregating tendency, thus maintaining high nonlinear optical efficiency. These results provided an insight for the structural control toward managing molecular and nanoscale aggregation phenomena of C_{60}-based starburst and dendritic suprastructures in the materials design of 2PA-based photonic devices and photodynamic therapeutics.

Acknowledgements

We thank Air Force Office of Scientific Research for funding under the contract number FA9550-05-1-0154.

Supporting information available

MALDI–TOF mass spectrum of C_{60}(>DPAF-C_9) **1**; comparison profiles of MALDI–TOF mass spectra among C_{60}(>DPAF-C_9), C_{60}(>DPAF-C_9)$_2$, and C_{60}(>DPAF-C_9)$_4$; MALDI–TOF mass spectrum of C_{60}(>DPAF-C_9)$_4$ **3b**; comparison of ^{13}C NMR spectra of C_{60}(>DPAF-C_9) and C_{60}(>DPAF-C_9)$_2$; the procedure of proton integration ratio measurement and the calculation of proton counts in ^{1}H NMR spectra of C_{60}(>DPAF-C_9), C_{60}(>DPAF-C_9)$_2$, and C_{60}(>DPAF-C_9)$_4$.

References

1. D. M. Guldi and M. Prato, *Acc. Chem. Res*., 2000, **33**, 69-73.
2. D. M. Guldi and P. V. Kamat, *"Fullerenes, Chemistry, Physics and Technology,"* ed. by K. M. Kadish and R. S. Ruoff, Wiely-Interscience, New York, 2000, pp. 225-281.

3. M. Maggini and D. M. Guldi, *"Molecular and Supramolecular Photochemistry,"* ed. by V. Ramamurthy and K. S. Schanze, Marcel Dekker, New York, 2000, Vol. 4, pp. 149-196.
4. C. Yu, T. Canteenwala, M. E. El-Khouly, Y. Araki, L. Y. Chiang, B. C. Wilson, O. Ito and K. Pritzker, *J. Mater. Chem*., 2005, **15**, 1857-1864.
5. C. Yu, T. Canteenwala, H. H. C. Chen, B. J. Chen, M. Canteenwala and L. Y. Chiang, *Proc. Electrochem. Soc*., 1999, **12**, 234-249.
6. C. Yu, T. Canteenwala, L. Y. Chiang, B. Wilson and K. Pritzker, *Synth. Met*., 2005, **153**, 37-40.
7. L. W. Tutt and A. Kost, *Nature*, 1992, **356**, 225-226.
8. D. G. McLean, R. L. Sutherland, M. C. Brant, D. M. Brandelik, P. A. Fleitz and T. Pottenger, *Opt. Lett*., 1993, **18**, 858-860.
9. T. H. Wei, T. H. Huang, T. T. Wu, P. C. Tsai and M. S. Lin, *Chem. Phys. Lett.*, 2000, **318**, 53-57.
10. Q. L. Zhou, J. R. Heflin, K. Y. Zamani-Khamiri and A. Garito, *Phys. Rev. A*, 1991, **43**, 1673.
11. A. Kost, L. W. Tutt, M. B. Klein, T. K. Dougherty and W. E. Elias, *Opt. Lett*., 1993, **18**, 334-336.
12. F. Z. Henari, K. H. Cazzini, D. N. Weldon and W. J. Blau, *Appl. Phys. Lett*., 1996, **68**, 619.
13. Y.-P. Sun and J. E. Riggs, *Int. Rev. Phys. Chem*., 1999, **18**, 43.
14. J. E. Riggs and Y.-P. Sun, *J. Phys. Chem. A*, 1999, **103**, 485-495.
15. Y. L. Song, G. Y. Fang, Y. X. Wang, S. T. Liu, C. F. Li, L. C. Song, Y. H. Zhu and Q. M. Hu, *Appl. Phys. Lett*., 1999, **74**, 332-334.
16. M. Maggini, C. D. Faveri, G. Scorrano, M. Prato, G. Brusatin, M. Guglielmi, M. Meneghetti, R. Signorini and R. Bozio, *Chem. Eur. J*., 1999, **5**, 2501-2510.
17. K. Dou and E. T. Knobbe, *J. Nonlin. Opt. Phys. Mater*., 2000, **9**, 269-287.
18. Z. B. Liu, J. G. Tian, W. P. Zang, W. Y. Zhou, C. P. Zhang, J. Y. Zheng, Y. C. Zhou and H. Xu, *Appl. Opt*., 2003, **42**, 7072-7076.
19. E. Koudoumas, M. Konstantaki, A. Mavromanolakis, S. Couris, M. Fanti, F. Zerbetto, K. Kordatos and M. Prato, *Chem. Eur. J*., 2003, **9**, 1529-1534.
20. G. Kopitkovas, A. Chugreev, J. F. Nierengarten, Y. Rio, J. L. Rehspringer and B. Honerlage, *Opt. Mater*., 2004, **27**, 285-291.
21. H. I. Elim, J. Quyang, S. H. Goh and W. Ji, *Thin Solid Films*, 2005, **477**, 63-72.
22. K. A. Drenser, R. J. Larsen, F. P. Strohkendl and L. R. Dalton, *J. Phys. Chem. A*, 1999, **103**, 2290-2301.
23. S. V. Rao, D. N. Rao, J. A. Akkara, B. S. DeCristofano and D. V. G. L. N. Rao, *Chem. Phys. Lett*., 1998, **297**, 491-498.
24. G. Banfi, D. Fortusini, M. Bellini and P. Milani, *Phys. Rev. B: Condensed Matter*, 1997, **56**, R10075-R10078.

25. L. Y. Chiang, P. A. Padmawar, T. Canteenwala, L.-S. Tan, G. S. He, R. Kannan, R. Vaia, T.-C. Lin, Q. Zheng and P. N. Prasad, *Chem. Comm*., 2002, 1854-1855.
26. P. A. Padmawar, T. Canteenwala, S. Verma, L.-S. Tan, G. S. He, P. N. Prasad and L. Y. Chiang, *Synth. Met*., 2005, **154**, 185-188.
27. Y. Zhao, Y. Shirai, A. D. Slepkov, L. Cheng, L. B. Alemany, T. Sasaki, F. A. Hegmann and J. M. Tour, *Chem. Eur. J*., 2005, **11**, 3643-3658.
28. P. A. Padmawar, J. O. Rogers, G. S. He, L. Y. Chiang, T. Canteenwala, L.-S. Tan, Q. Zheng, C. Lu, J. E. Slagle, E. Danilov, D. G. McLean, P. A. Fleitz and P. N. Prasad, *Chem. Mater*., 2006, **18**, 4065-4074.
29. B. Z. Tang, H. Xu, J. W. Y. Lam, P. P. S. Lee, K. Xu, Q. Sun and K. K. L. Cheuk, *Chem. Mater*., 2000, **12**, 1446-1455.
30. P. A. Padmawar, T. Canteenwala, L.-S. Tan and L. Y. Chiang, *J. Mater. Chem*., 2006, **16**, 1366-1378.
31. H. Luo, M. Fujitsuka, Y. Araki, O. Ito, P. Padmawar and L. Y. Chiang, *J. Phys. Chem. B,* 2003, **107**, 9312-9318.
32. T. W. Ebbesen, K. Tanigaki and S. Kuroshima, *Chem. Phys. Lett*., 1991, **181**, 501-504.
33. For a review of 2PA-active materials: T. C. Lin, S. J. Chung, K. S. Kim, X. Wang, G. S. He, J. Swiatkiewicz, H. E. Pudavan and P. N. Prasad, *Adv. Polym. Sci*., 2003, **161**, 157-193.
34. G. S. He, J. D. Bhawalkar, C. F. Zhao and P. N. Prasad, *Appl. Phys. Lett*., 1995, **67**, 2433-2435.
35. J. E. Ehrlich, X. L. Wu, L.-Y. Lee, Z.-Y. Hu, H. Roeckel, S. R. Marder and J. W. Perry, *Opt. Lett***.,** 1997, **22**, 1843-1845.
36. M. G. Silly, L. Porres, O. Mongin, P-A. Chollet and M. Blanchard-Desce, *Chem. Phys. Lett*., 2003, **379**, 74-80.
37. W. R. Dichtel, J. M. Serin, C. Edder, J. M. J. Frechet, M. Matuszewski, L. S. Tan, T. Y. Ohulchanskyy and P. N. Prasad, *J. Am. Chem. Soc*., 2004, **126**, 5380-5381.
38. P. A. Padmawar, T. Canteenwala, S. Verma, L.-S. Tan and L. Y. Chiang, *J. Macromol. Sci. A, Pure Appl. Chem*., 2004, **41**, 1387-1400.
39. M. Sheik-Bahae, A. A. Said, T. Wei, D. J. Hagan and E. W. Van Stryland, *IEEE J. Quantum Electron,* 1990, **26**, 760.
40. Q. Ying, J. Marecek and B. Chu, *Chem. Phys. Lett*., 1994, **219**, 214.
41. R. V. Hongchuck, T. W. Cruger and J. Milliken, *J. Am. Chem. Soc*., 1993, **115**, 3034.
42. L. A. Bulavin, I. I. Adamenko, V. M. Yashchuk, T. Yu, Ogul'chansky, Y. I. Prylutskyy, S. S. Durov and P. Scharff, *J. Mol. Liq*., 2001, **93**, 187-191.
43. L. B. Justus, Z. H. Kafafi and A. L. Huston, *Opt. Lett*., 1993, **18**, 1603.

44. R. A. Ganeev, A. I. Ryasnyansky, N. Ishizawa, M. Baba, M. Suzuki, M. Turu, S. Sakakibara and H. Kuroda, *Opt. Commun*., 2004, **231**, 431-436.

45. H. I. Elim, J. Y. Ouyang, J. He, S. H. Goh, S. H. Tang and W. Ji, *Chem. Phys. Lett*., 2003, **369**, 281.

46. H. I. Elim, W. Ji, G. C. Meng, J. Y. Ouyang and S. H. Goh, *J. Nonlinear Opt. Phys*., 2003, **12**, 175.

Table 1. Two-photon absorption cross-section values ($\sigma_2 = \beta\hbar\omega/N$) of C_{60}(>DPAF-C_9)$_x$ (x = 1, 2, or 4) and the sum of their individual molecular components, measured at 780 nm with 150-fs laser pulses and I = 163 GW/cm^2.

Chromophore /solvent	[*C*] (M)	β (cm/GW)	σ_2 ($\times 10^{-48}$ cm^4.sec.photon^{-1}.molecule^{-1})	$\sigma_{2,adj}$ ($\times 10^{-48}$ cm^4.sec.photon^{-1}.molecule^{-1})[a]	$\Delta\sigma_{2,adj}$ ($\times 10^{-48}$ cm^4.sec.photon^{-1}.molecule^{-1})
CS_2		0.03			
C_{60} + 1 [CH_3(DPAF-C_9)]	1.0×10^{-4}	0.033	12.7	9.3	
C_{60}(>DPAF-C_9) **1**/CS_2	1.0×10^{-4}	0.036	25.3	**21.9**	
	1.86×10^{-3}	0.080	11.4	8.0	13.9
	1.0×10^{-2}	0.100	2.9	0.3	7.7
C_{60} + 2 [CH_3(DPAF-C_9)]	1.0×10^{-4}	0.037	29.6	26.2	
C_{60}(>DPAF-C_9)$_2$ **2**/CS_2	1.0×10^{-4}	0.041	46.4	**43.0**	
	1.86×10^{-3}	0.088	13.2	9.8	33.2
	1.0×10^{-2}	0.130	4.2	0.8	9.0
C_{60} + 4 [CH_3(DPAF-C_9)]	1.0×10^{-4}	0.041	46.4	43.0	
C_{60}(>DPAF-C_9)$_4$ **3a**/CS_2	1.0×10^{-4}	0.051	88.6	**85.2**	
	1.86×10^{-3}	0.120	20.4	17.0	68.2
	1.0×10^{-2}	0.280	10.5	7.1	9.9
C_{60}(>DPAF-C_9)$_4$ **3b**/CS_2	1.0×10^{-4}	0.045	63.3	**59.9**	
	1.86×10^{-3}	0.097	15.2	11.8	48.1
	1.0×10^{-2}	0.160	5.5	2.1	9.7

[a] Calibrated σ_2 values to the reported data collected at 1.0×10^{-2} M using a lower laser energy source of 10–30 GW/cm^2.[28]

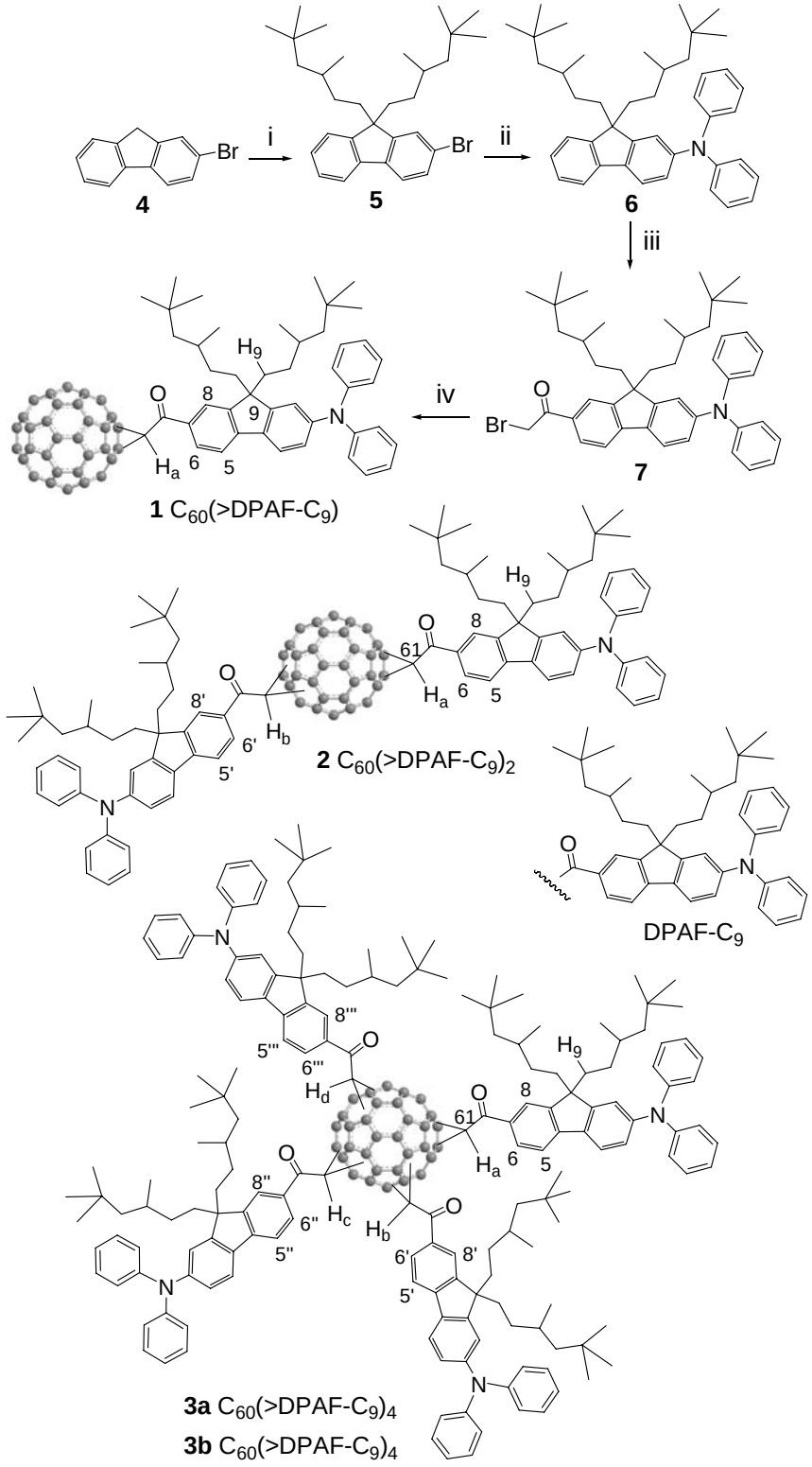

Scheme 1. *Reagents and conditions:* i. $(CH_3)_3CCH_2CH(CH_3)CH_2CH_2$-OMs, *t*-BuOK, THF, 10 °C–rt, 15 h; ii. diphenylamine, tris(dibenzylideneacetone)dipalladium(0) (cat.), *rac*-BINAP (cat.), *t*-BuONa, toluene, reflux, 8.0 h; iii. bromoacetyl bromide, $AlCl_3$, $ClCH_2CH_2Cl$, 0 °C to rt, 8.0 h; iv. C_{60}, DBU, toluene, rt, 5.0 h.

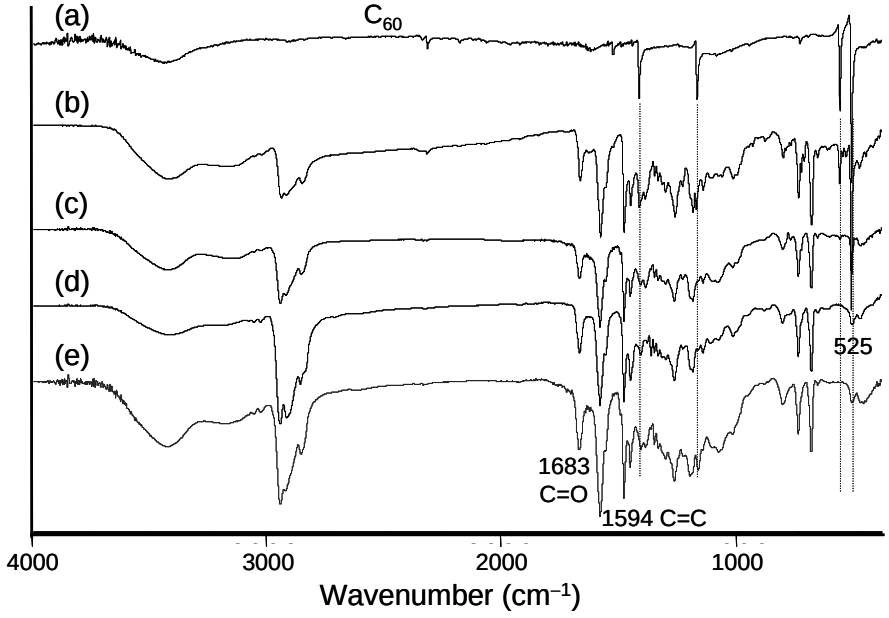

Fig. 1. Infrared spectra of (a) pure C_{60}, (b) C_{60}(>DPAF-C_9) **1**, (c) C_{60}(>DPAF-C_9)$_2$ **2**, (d) C_{60}(>DPAF-C_9)$_4$ **3a**, and (e) C_{60}(>DPAF-C_9)$_4$ **3b**, all showing a nearly identical characteristic carbonyl absorption band at 1683 cm^{-1} largely shifted from 1720 cm^{-1}.

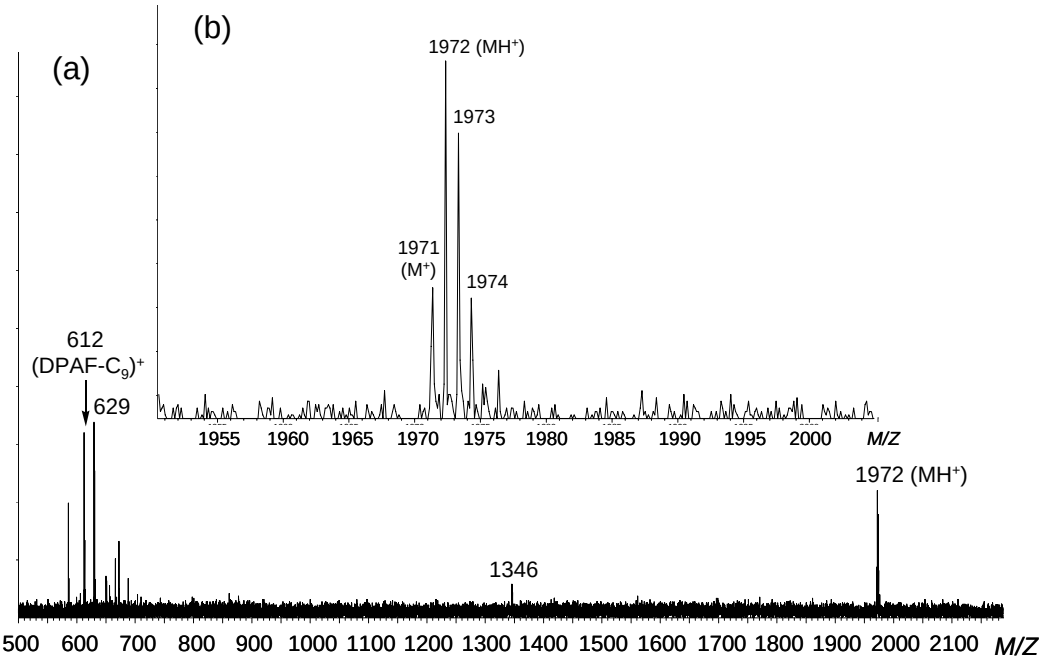

Fig. 2. Positive ion MALDI-TOF mass spectra of the bisadduct C_{60}(>DPAF-C_9)$_2$ **2**.

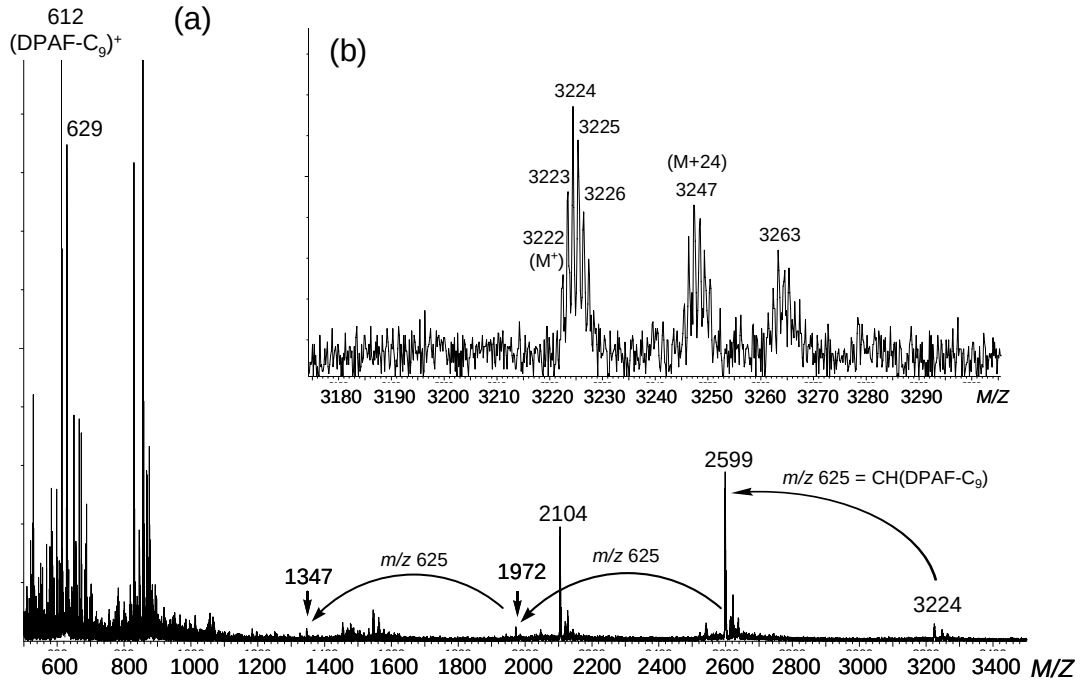

Fig. 3. Positive ion MALDI-TOF mass spectra of the tetraadduct C_{60}(>DPAF-C_9)$_4$ **3a**.

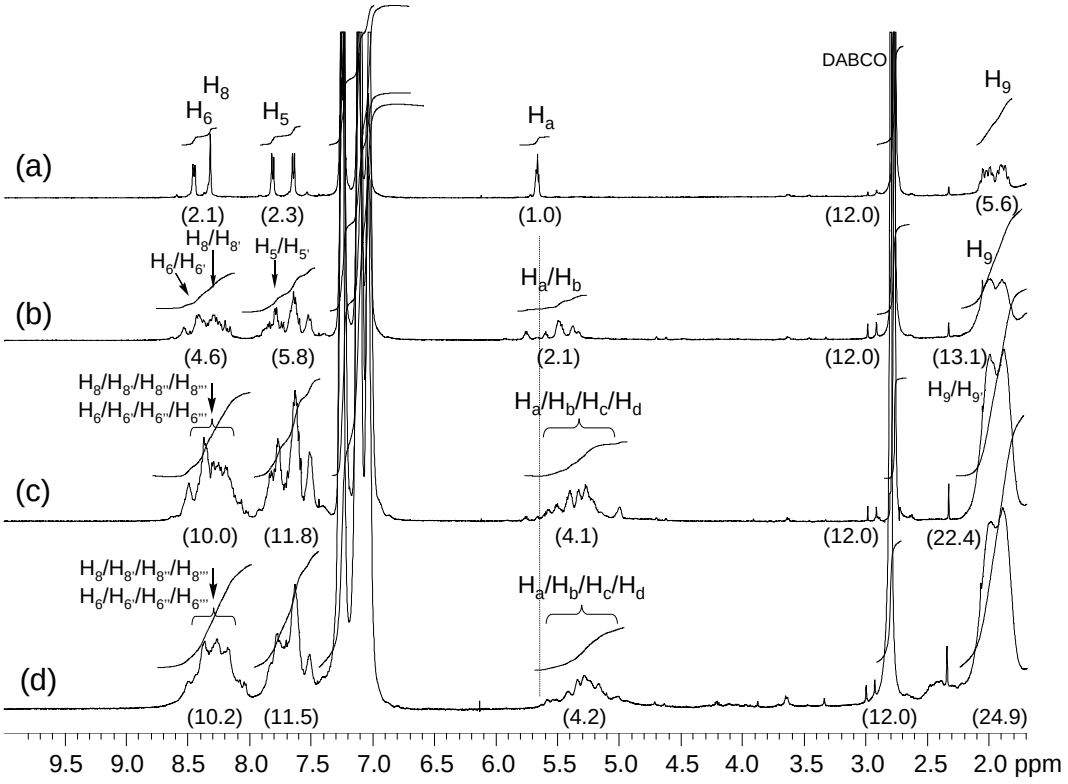

Fig. 4. ^{1}H NMR spectra of (a) C_{60}(>DPAF-C_9) **1**, (b) C_{60}(>DPAF-C_9)$_2$ **2**, (c) C_{60}(>DPAF-C_9)$_4$ **3a**, and (d) C_{60}(>DPAF-C_9)$_4$ **3b** in $CDCl_3$ with relative integration values, which were calibrated by the use of an internal DABCO standard in the same concentration among (a)–(d), indicated in parenthesis.

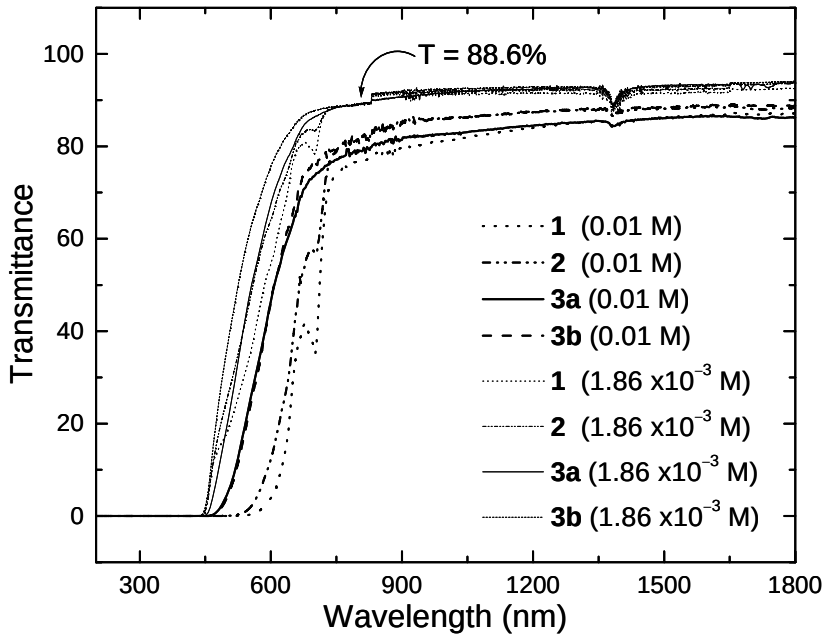

Fig. 5. UV-Vis-NIR transmission spectra of CS_2, C_{60}(>DPAF-C_9) **1**, C_{60}(>DPAF-C_9)$_2$ **2**, C_{60}(>DPAF-C_9)$_4$ **3a**, and C_{60}(>DPAF-C_9)$_4$ **3b**, with the latter four compounds dissolved in CS_2 in a concentration indicated.

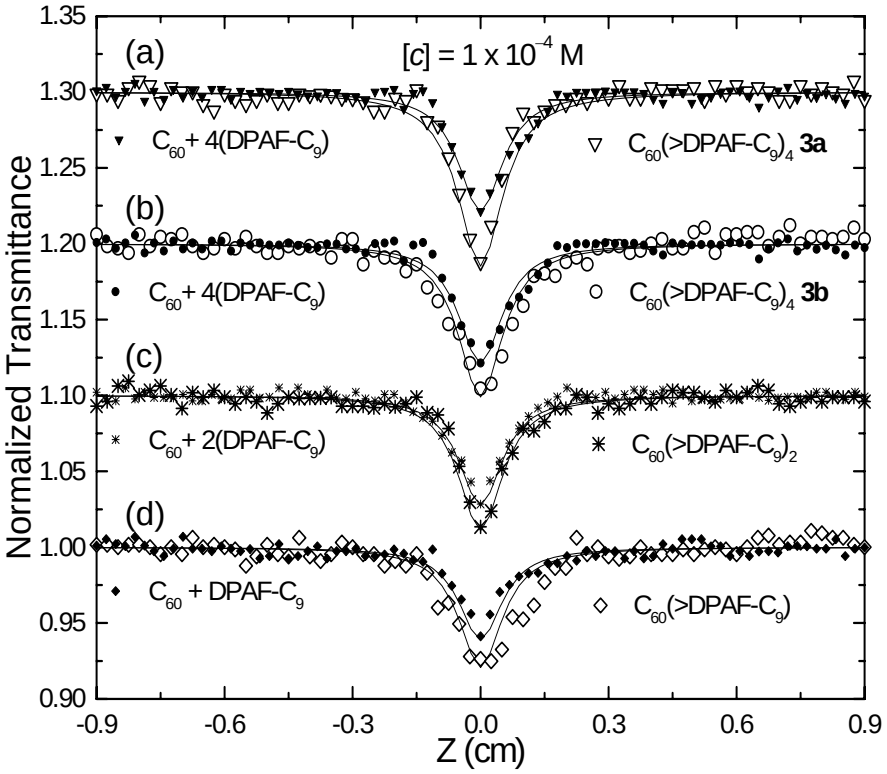

Fig. 6. Open-aperture *Z*-scans of 1-mm-thick solution of (a)/(b) C_{60}(>DPAF-C_9)$_4$, (c) C_{60}(>DPAF-C_9)$_2$, and (d) C_{60}(>DPAF-C_9) in CS_2 in comparison with the sum of individual model components [C_{60} and CH_3(DPAF-C_9)], performed at the same concentration of 1.0×10^{-4} M and irradiance of 163 GW/cm^2. The data are vertically shifted for clear presentation. Solid lines are the theoretical fit for two-photon absorption.

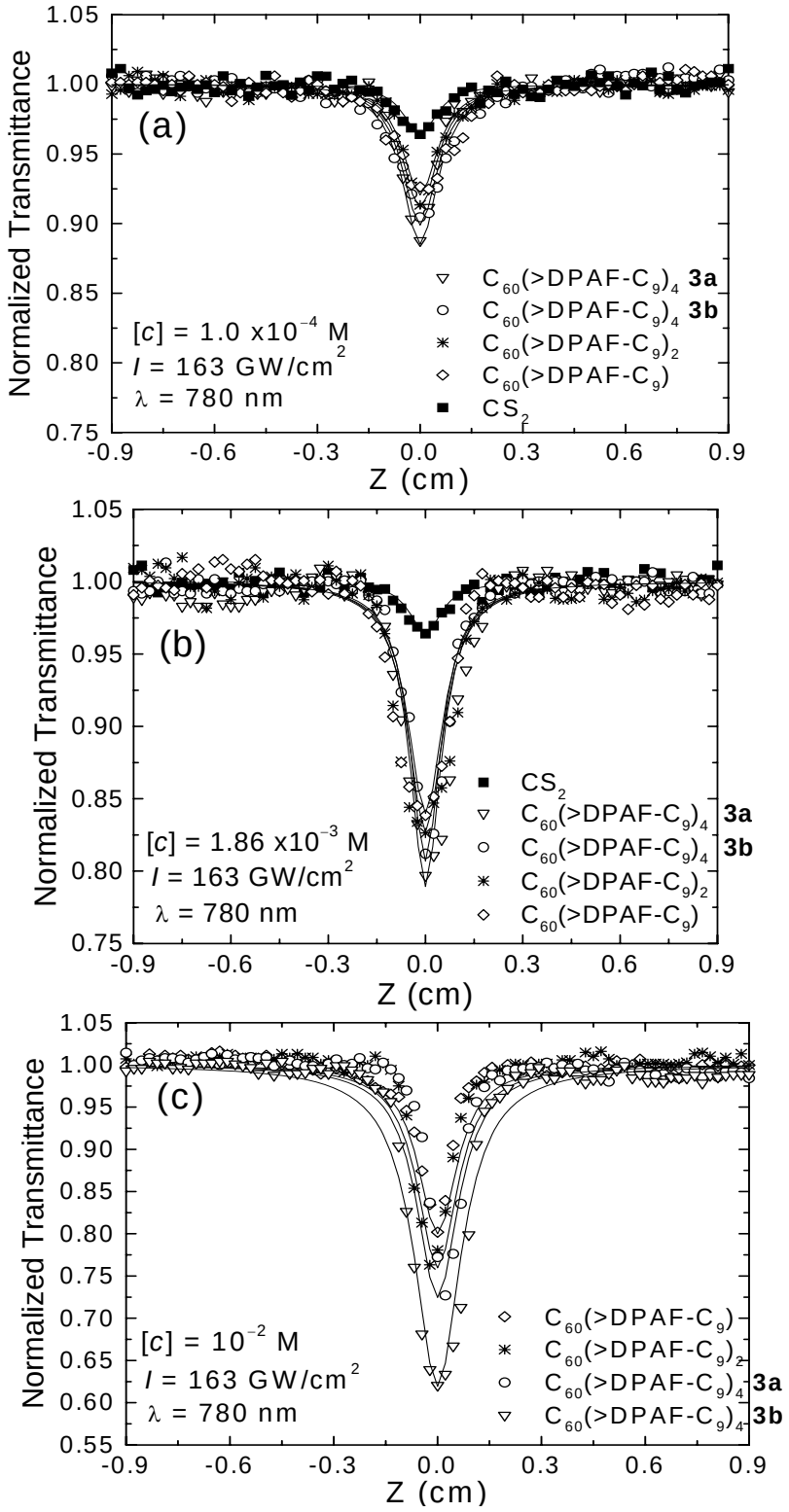

Fig. 7. Open-aperture *Z*-scans of 1-mm-thick solution of C_{60}(>DPAF-C_9), C_{60}(>DPAF-C_9)$_2$, and C_{60}(>DPAF-C_9)$_4$ in CS_2 performed at different concentrations of (a) 1.0×10^{-4}, (b) 1.86×10^{-3}, and (c) 1.0×10^{-2} M with irradiance of 163 GW/cm^2. Solid lines are the theoretical fit for two-photon absorption.

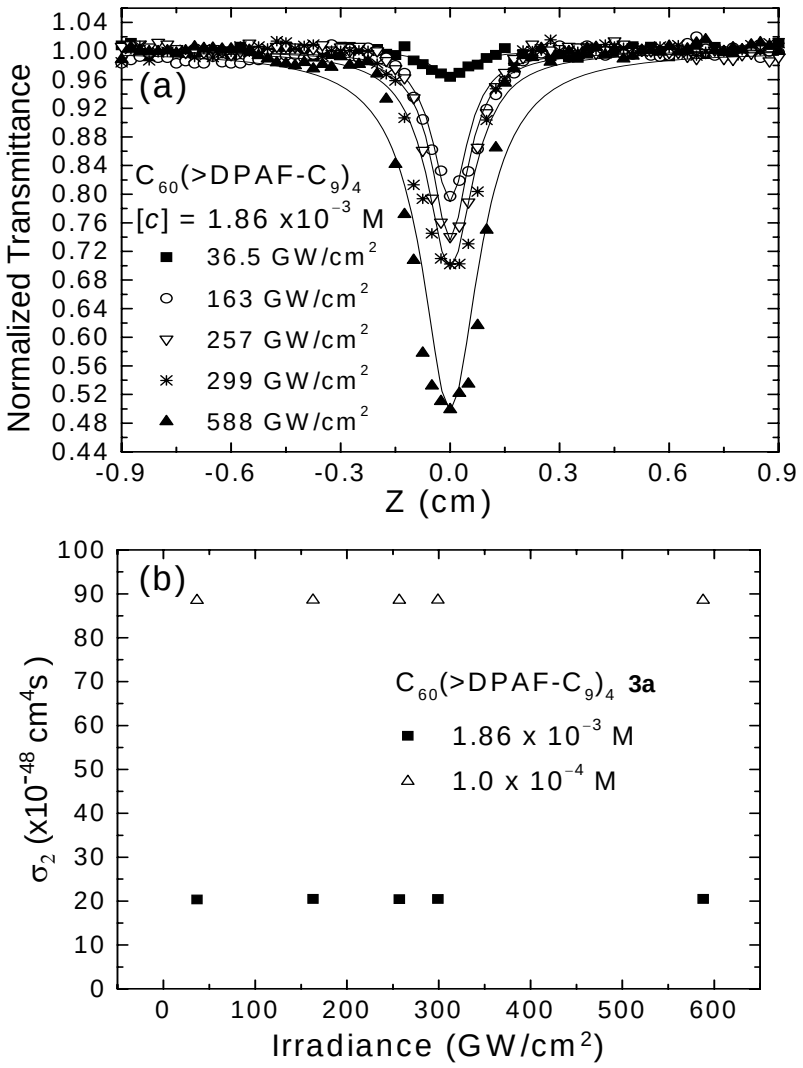

Fig. 8. (a) Open-aperture *Z*-scans at different excitation irradiances for C_{60}(>DPAF-C_9)$_4$ **3a** with experimental data presented as scatter graphs and fitting curves, calculated by *Z*-scan theory,[38] as solid lines and (b) irradiance independence of the σ_2 profile of **3a** in two concentrations indicated.

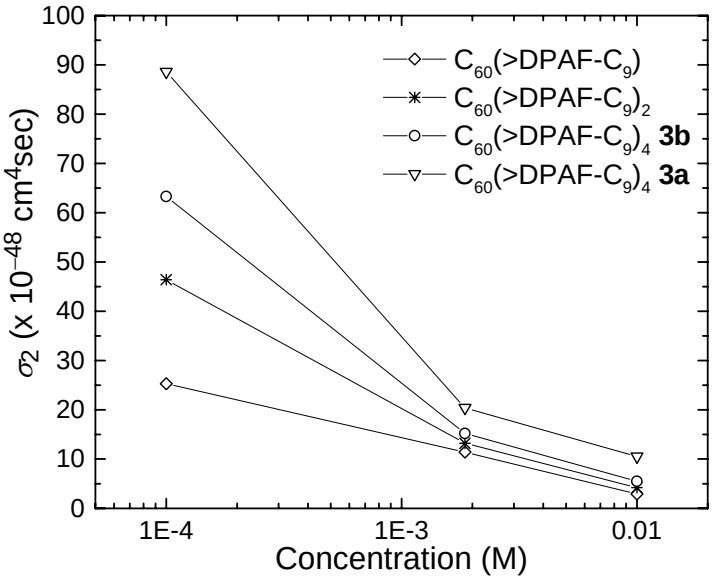

Fig. 9. Concentration dependence of 2PA cross section values σ_2 of C_{60}(>DPAF-C_9), C_{60}(>DPAF-C_9)$_2$, and C_{60}(>DPAF-C_9)$_4$ in CS_2.

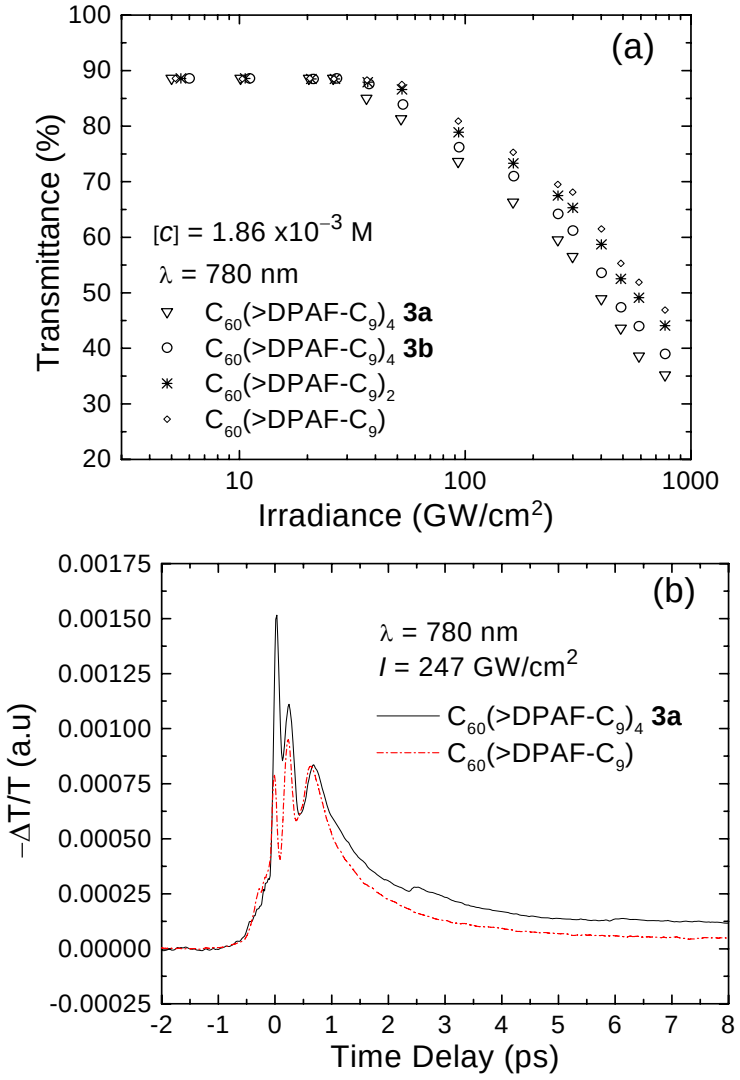

Fig. 10. (a) Nonlinear transmission of C_{60}(>DPAF-C_9), C_{60}(>DPAF-C_9)$_2$, and C_{60}(>DPAF-C_9)$_4$ in CS_2 and (b) the measurement of transient transmission change ($-\Delta T/T$) in the solution of C_{60}(>DPAF-C_9) and **3a**. All the measurements were conducted with 150 fs laser pulses at λ = 780 nm. All four samples showed the nearly identical linear transmission T = 88.6% in an optical path of 1 mm.